
Research Article: Methods/New Tools / Novel Tools and Methods

Uncovering Neuronal Networks Defined by Consistent between-Neuron Spike Timing from Neuronal Spike Recordings

Roemer van der Meij¹ and Bradley Voytek^{1,2,3,4}

¹Department of Cognitive Science, University of California, San Diego, La Jolla, CA 92093, USA

²Neurosciences Graduate Program, University of California, San Diego, La Jolla, CA 92093, USA

³Halicioglu Data Science Institute, University of California, San Diego, La Jolla, CA 92093, USA

⁴Kavli Institute for Brain and Mind, University of California, San Diego, La Jolla, CA 92093, USA

DOI: 10.1523/ENEURO.0379-17.2018

Received: 7 November 2017

Revised: 1 April 2018

Accepted: 21 April 2018

Published: 8 May 2018

Author contributions: R.v.d.M. and B.V. designed research; R.v.d.M. performed research; R.v.d.M. contributed unpublished reagents/analytic tools; R.v.d.M. analyzed data; R.v.d.M. and B.V. wrote the paper.

Funding: <http://doi.org/10.13039/100000025HHS> | NIH | National Institute of Mental Health (NIMH)
MH095984-03S1

Funding: <http://doi.org/10.13039/10000001> National Science Foundation (NSF)
1736028

Funding: <http://doi.org/10.13039/100007911UC> | University of California, San Diego (UCSD)

Funding: <http://doi.org/10.13039/100000879> Alfred P. Sloan Foundation

Conflict of Interest: Authors declare no conflicts of interest.

Correspondence to: Roemer van der Meij, Cognitive Science, University of California, San Diego, La Jolla, CA 92093, USA. E-mail: roemer.van.der.meij@gmail.com

Cite as: eNeuro 2018; 10.1523/ENEURO.0379-17.2018

Alerts: Sign up at eneuro.org/alerts to receive customized email alerts when the fully formatted version of this article is published.

Accepted manuscripts are peer-reviewed but have not been through the copyediting, formatting, or proofreading process.

1 Title: Uncovering neuronal networks defined by consistent between-neuron spike timing
2 from neuronal spike recordings

3

4 Abbreviated title: Uncovering spike timing networks from neuronal recordings

5

6 Roemer van der Meij¹, Bradley Voytek^{1,2,3,4}

7

8 ¹Department of Cognitive Science, University of California, San Diego, La Jolla, CA 92093, USA.

9 ²Neurosciences Graduate Program, University of California, San Diego, La Jolla, CA 92093, USA.

10 ³Halicioglu Data Science Institute, University of California, San Diego, La Jolla, CA 92093, USA.

11 ⁴Kavli Institute for Brain and Mind, University of California, San Diego, La Jolla, CA 92093, USA.

12

13 Correspondence to: Roemer van der Meij, Cognitive Science, University of California, San Diego, La Jolla,
14 CA 92093, USA. E-mail: roemer.van.der.meij@gmail.com

15

16 Number of figures: 7

17 Number of tables: 0

18 Number of multimedia: 0

19

20 Numbers of words in Abstract: 248

21 Numbers of words in Introduction: 746

22 Numbers of words in Discussion: 1784

23

24 Acknowledgements: We thank S.R. Cole, T. Donoghue, R. Gao, E. Peterson, and T. Tran for their
25 discussions and comments, and especially E. Maris for discussions on the project's premise years ago.

26 Both R.v.d.M. and B.V. were supported by the National Institute of Mental Health (MH095984-03S1) and
27 University of California, San Diego, and B.V. was additionally supported by a Sloan Research Fellowship
28 and the National Science Foundation (1736028).

29

30 Conflicts of interest: The authors declare no competing financial interests.

31

32 **Abstract**

33

34 It is widely assumed that distributed neuronal networks are fundamental to the functioning of the brain.
35 Consistent spike timing between neurons is thought to be one of the key principles for the formation of
36 these networks. This can involve synchronous spiking or spiking with time delays, forming spike
37 sequences when the order of spiking is consistent. Finding networks defined by their sequence of time-
38 shifted spikes, denoted here as spike timing networks, is a tremendous challenge. As neurons can
39 participate in multiple spike sequences at multiple between-spike time delays, the possible complexity
40 of networks is prohibitively large. We present a novel approach that is capable of (1) extracting spike
41 timing networks regardless of their sequence complexity, and (2) that describes their spiking sequences
42 with high temporal precision. We achieve this by decomposing frequency-transformed neuronal spiking
43 into separate networks, characterizing each network's spike sequence by a time delay per neuron,
44 forming a spike sequence timeline. These networks provide a detailed template for an investigation of
45 the experimental relevance of their spike sequences. Using simulated spike timing networks, we show
46 network extraction is robust to spiking noise, spike timing jitter, and partial occurrences of the involved
47 spike sequences. Using rat multi-neuron recordings, we demonstrate the approach is capable of
48 revealing real spike timing networks with sub-millisecond temporal precision. By uncovering spike timing
49 networks, the prevalence, structure, and function of complex spike sequences can be investigated in
50 greater detail, allowing us to gain a better understanding of their role in neuronal functioning.

51

52

53 **Significance statement**

54

55 Spike timing consistencies in neuronal networks are widely thought to be one of several key principles
56 behind neuronal functioning. They are challenging to investigate, however, because there is effectively
57 an infinite number of combinations of neurons and their between-neuron time delays for any given
58 recording. Many techniques have been developed for their analysis, but they are still limited by the
59 complexity of spike timing patterns they can reveal. Here we present a novel approach that can reveal
60 spike timing patterns with arbitrary combinatorial complexity. This provides a new opportunity for
61 investigating spike timing networks, which is crucial to gain a better understanding of the role they play
62 in neuronal functioning.

63

64 **Introduction**

65

66 Distributed networks of neurons, or cell assemblies, are widely assumed to be fundamental to brain
67 functioning (Hebb, 1949; Treisman, 1996; Singer, 1999; Varela et al., 2001; Harris, 2005; Buzsaki, 2010).
68 A subset of these networks is thought to be formed by consistent timing of action potentials, or spikes,
69 between neurons (Bienenstock, 1995; Singer, 1999; Ainsworth et al., 2012; Feldman, 2012), a feature of
70 spike recordings across species (Mainen and Sejnowski, 1995; Salinas and Sejnowski, 2001; VanRullen et
71 al., 2005; Fujisawa et al., 2008; Ratté et al., 2013). The spiking between neurons of such networks can be
72 synchronous or involve time delays (Izhikevich, 2006; Fujisawa et al., 2008; Sakurai et al., 2013), forming
73 spike sequences when firing in a consistent order (Lee and Wilson, 2002; Ikegaya et al., 2004; Tiesinga et
74 al., 2008). Spike sequences can involve the same neurons and occur within the same time window (Mao
75 et al., 2001; MacLean et al., 2005; Luczak et al., 2007; Matsumoto et al., 2013; Miller et al., 2014).
76 Though there is still much debate about how important spike timing is in comparison to alternatives
77 such as rate-based coding schemes (Kumar et al., 2010; Rolls and Treves, 2011; Ainsworth et al., 2012),
78 the investigation of spike timing networks and their spike sequences remains necessary to further our
79 understanding of basic neuronal operations.

80 Finding networks defined by their sequences of consistent time-shifted spikes between neurons,
81 denoted in the following as *spike timing networks*, is a tremendous challenge due to their possible
82 complexity, as neurons can participate in multiple spike sequences at a continuum of between-spike
83 time delays. The past decades have seen the arrival of many methods that can characterize spike timing
84 networks (Abeles and Gerstein, 1988; Nadasdy et al., 1999; Chapin and Nicolelis, 1999; Tetko and Villa,
85 2001; Grün et al., 2002; Lee and Wilson, 2002; Schnitzer and Meister, 2003; Ikegaya et al., 2004; Okatan
86 et al., 2005; Schneider et al., 2006; Nikolic, 2007; Pipa et al., 2008; Schrader et al., 2008; Berger et al.,
87 2010; Louis et al., 2010; Peyrache et al., 2010; Eldawlatly et al., 2010; Humphries, 2011; Lopes-dos-
88 Santos et al., 2011; Gansel and Singer, 2012; Torre et al., 2016). Their application has led to important
89 insights, yet they have several limitations, especially when it comes to their application on large scale
90 neuronal recordings (Buzsaki, 2004). Namely, either: (1) the complexity of the identified networks is
91 limited due to combinatorial explosion with increasing network size (e.g. template searching), (2) the
92 networks are described only by the association of their member neurons without describing spike
93 sequences, (3) between-spike time delays greater than 0 are either discarded or not recovered, (4)
94 temporal binning of spike times leads to reduced temporal precision, (5) networks with overlapping
95 member neurons are not separated, or, (6) a combination of the above. Though not important for every
96 investigation of interactions in spiking networks (e.g., for higher order interactions see Nakahara and
97 Amari, 2002; Yu et al., 2009; Eldawlatly et al., 2010; Staude et al., 2010; Balaguer-Ballester et al., 2011;
98 Shimazaki et al., 2012), they are essential for the exact identification of neurons and their spike
99 sequences, and investigating their occurrence as a function of experimental variables.

100 We present a novel approach for revealing spike timing networks that does not suffer from the
101 above problems. The key features of our approach, are that (1) it can find networks regardless of the
102 complexity of their spiking sequences, and that (2) it describes these sequences with sub-millisecond
103 precision by a time coefficient per neuron (per sequence; see Fig 1). This is achieved by applying a
104 method developed for electrophysiological recordings (intended for revealing phase-coupled oscillatory
105 networks, such as traveling waves; van der Meij et al., 2015), on the spectral covariance (or, *cross*
106 *spectra*) obtained from a spectral analysis of discrete neuronal spiking time series. In these cross
107 spectra, consistent between-neuron spike time delays are described by linearly increasing phase
108 differences over frequencies. The method finds networks and their spike sequences by their unique
109 patterns of between-neuron phase differences over frequencies and trials (epochs). In the following, we
110 first show that our approach is capable of recovering simulated spike timing networks and their
111 sequences under various noise conditions, and then provide a proof-of-concept by showing networks

112 extracted from rat hippocampus and medial prefrontal cortex (Fujisawa et al., 2008, 2014), which
113 reflected peak cross-correlogram time delays with high accuracy. Together, this demonstrates that our
114 approach is a robust method for revealing and characterizing spike timing networks in neuronal
115 recordings.
116

117 **Materials and Methods**

118

119 **1. Extracting spiking timing networks from neuronal spike recordings**

120 Spike timing consistency between neurons is thought to be a key feature of neuronal spike recordings.
121 In the following, we describe how a novel application of a recent technique, (SPACE; van der Meij et al.,
122 2015, 2016) can be used to find sequences of consistent time-shifted spikes between neurons, denoted
123 in the following as spike timing networks, in large scale neuronal spike recordings, without a priori
124 information about the involved neurons and their timing. Below we illustrate the procedure for
125 extracting spike timing networks (with details in dedicated sections), and how to interpret their
126 characterization.

127 We start with any kind of multi-electrode neuronal recording over time t of which neurons J and
128 their spikes have been identified (using e.g. Rossant et al., 2016). Suppose our recording contains 2
129 groups of 3 neurons that have consistent between-neuron spike timing (i.e., spike timing networks, Fig
130 1A blue/green, Fig 1B), embedded in other spiking activity. The blue network has a spiking sequence of
131 neuron 3 to 4 to 5 with a timeline of 0ms-1ms-2ms, leading to consistent spike time delays of 1ms for
132 pairs 3-4 and 4-5, and a 2ms delay of 3-5. The green network has the same pattern but for neurons 5, 6,
133 and 7. If cross-correlograms would be computed from the neuronal spike recordings (Fig 1B), they would
134 have peaks at 1ms for neuron pairs 3-4, 4-5, 5-6, 6-7, at -1ms for pair 4-3, 5-4, 6-5, 7-6, at 2ms for pair 3-
135 5, 5-7, and at -2ms for pair 5-3, 7-5. How often the sequences of the blue and green networks occur,
136 depends on two experimental conditions. The blue networks occur once per trial of condition A and
137 twice for those of B, (Fig 1C), the green network vice versa.

138 To extract a parsimonious description of the above networks, we arrange the detected spikes in
139 neuron-by-time ($J \times t$) binary matrices S_l (1 = spike, 0 = no spike; Fig 1C), per trial l of the experiment (or
140 any other meaningful temporal segmentation; throughout the text, J refers to neurons, K to
141 frequencies, L to trials). Then, we obtain 'cross spectra' from these trial-specific matrices. To achieve
142 this, we first convolve the matrices S_l with complex exponentials (Fig 1, Step 1) at multiple frequencies
143 k , resulting in frequency-specific and trial-specific complex-valued neuron-by-time ($J \times t$) matrices Z_{kl} .
144 Subsequently, we compute the cross products $Z_{kl}Z_{kl}^*$ of these matrices over time (Fig 1, Step 2; $*$ =
145 complex conjugate transpose), resulting in complex-valued frequency-specific and trial-specific neuron-
146 by-neuron ($J \times J$) matrices X_{kl} : the cross spectra (Fig 1D). The choice of complex exponentials
147 determines key aspects of the spike timing networks and their extraction, and is discussed in detail in
148 Materials and Methods section 3. Having obtained the cross spectra, we should apply a neuron-wise
149 and/or trial-wise normalization (Fig 1, Step 3; see Materials and Methods section 4). After normalization,
150 we then extract spike timing networks using SPACE (Fig 1E, Step 4; which involves estimating the
151 number of networks to extract, see Materials and Methods section 2).

152 Spike timing networks, when defined by their discrete spiking sequences characterized as time-
153 shifted copies of spikes between neurons, can be extracted from the cross spectra, because the phases
154 of the off-diagonal elements of the cross spectra contain the consistent time delays between time-
155 shifted copies of spikes. The crucial principle here, is that the time difference between two binary spikes
156 in the time domain translates to phase differences in the frequency domain, linearly increasing with
157 frequency. That is, a 1ms time delay equals 1/20th of a cycle at 50Hz, 1/10th at 100Hz, 1/5th at 200Hz, etc.
158 (for types of spiking interactions other than time-shifted copies of spikes, see Lindemann et al., 2001).
159 The extraction technique uses this property to find the time delays between time-shifted copies of
160 neuronal spikes that explains the most variance in the cross spectra.

161 SPACE describes the cross spectra by multiple networks, each network consisting of three
162 parameter vectors (Fig 1E): the *neuron profile* ($1 \times J$), the *time profile* ($1 \times J$), and the *trial profile* ($1 \times L$).
163 The neuron profile describes how strongly each neuron is part of the network, by a single number per
164 neuron. The neuron profile of the blue network has high values for neurons 3, 4, and 5, and low values

165 for all other neurons. That is, only neurons 3 to 5 are part of this network. Due to their similar weighting,
166 neurons 3 to 5 likely have similar firing rates, and similar number of spike sequence' spikes. If another
167 neuron would have half the weighting, it will likely have either twice as many total spikes, or only fires in
168 half of the network's spike sequences (e.g., a sequence of neuron 3-4-5 in half of the trials, and 3-4 in
169 the rest). Note, it is possible for the neuron profile to have non-zero loadings for only one neuron, see
170 Materials and Methods section 4 for a discussion. The time profile describes the spike sequence of the
171 network, by a single time coefficient per neuron. Because the neuron profile of the blue network only
172 strongly involves neurons 3 to 5, only these coefficients of the time profile are meaningful. The time
173 profile of neurons 3 to 5 directly reflects the timeline of the spike sequence, 0ms-1ms-2ms. A crucial
174 observation here, is that all the temporal relationships at the level of neuron-pairs are described at the
175 level of individual neurons by the network's neuron profile (relationship strength) and time profile (spike
176 sequence timing). The above is the same for the green network. Importantly, if the blue and green spike
177 sequences occur at random intervals between them, the blue and green networks can be separated, as
178 there are no consistent relationships between neurons 3, 4, and neurons 6, 7. If the blue and green
179 spike sequences occurred at consistent intervals, they would both be captured by one network. This is
180 not surprising, as the above means there is, in fact, only one spike sequence. In the schematic of Figure
181 1, there is also a difference in how often a sequence of each network occurs in each condition, which
182 can be reflected by the trial profiles. Here, the weights for trials of the blue network reflect the *ratio* of
183 spike sequences in each trial of the two conditions, i.e. a trial loading that is twice as large for B as it is
184 for A. Importantly, the trial profile can provide a convenient way to investigate differences in spike time
185 consistency at the level of networks, instead of the level of neuron-pairs. For example, the difference
186 between two conditions can be investigated by comparing the means of the condition-specific trial
187 profile weights, or variations of trial profile weights can be related to other variables (e.g., reaction
188 times, parametric stimulus manipulations, etc.). Though in principle possible, the trial profile can be
189 noise sensitive (see the Results and Discussion sections). Additionally, the absence of an extracted
190 network is not evidence of a network's absence (in the recording), various reasons can prohibit a
191 network to not be found (e.g., noise, see Results and Discussion sections). Finally, see Materials and
192 Methods section 2 on how to compare values between and within the above profiles.

193 When interpreting the network profiles, it is crucial to keep in mind that they are estimated to
194 maximally explain the cross spectra (see Materials and Methods section 2). As such, anything that
195 affects the phase coupling patterns in the cross spectra, affects the profiles accordingly. For example, in
196 case a neuron spikes in a spike sequence of a network in some trials, but not in others, then the phase
197 coupling strength between this neuron and the others of the network will be weaker (or zero) in the
198 cross spectra for the latter trials compared to the former. Consequently, the neuron profile of this
199 network will have a lower weight for this neuron than for the others, and the trial profile will have lower
200 weights for those trials in which it didn't spike.

201 **2. SPACE describes time consistency induced phase coupling in cross spectra**

202 SPACE is a decomposition technique that describes the structure of phase coupling in cross spectra by
203 time delays between neurons (or electrodes/sensors/sites). The technique was developed for finding
204 oscillatory phase coupling structure (e.g., traveling waves) in electrophysiological recordings (van der
205 Meij et al., 2015, 2016), a type of data of which the frequency content itself is of primary interest. This
206 contrasts with the application we present here, for which this is not the case. The frequencies of the
207 used spectral transform are artificial and are chosen only such that they provide an accurate description,
208 via the networks SPACE extracts, of the temporal structure in discrete neural spike timing time series
209 (see Materials and Methods section 3). Apart from the manner of constructing the cross spectra, the
210 usage of the method in the current approach is identical to that in the original publication (referred to as
211 SPACE-time therein). The algorithm behind the method is extensively treated in its original publication

213 (van der Meij et al., 2015, but see also van der Meij et al., 2016 for an alternate presentation), and only
 214 elements essential to its current use will be mentioned here. Briefly, the technique consists of an
 215 Alternating Least Squares (ALS) algorithm to find the least squares estimates of its decomposition
 216 model. The element-wise formulation of this model for the cross spectra can be expressed as:

$$217 X_{j_1 j_2 k l} = \sum_{f=1}^F (a_{j_1 f} \cdot a_{j_2 f}) \cdot \exp(i2\pi\varphi_k(\sigma_{j_1 f} - \sigma_{j_2 f})) \cdot b_{k f}^2 \cdot c_{l f}^2 + \varepsilon_{j_1 j_2 k l}$$

218 The complex-valued cross spectrum ($X_{j_1 j_2 k l}$) of neuron pair j_1 and j_2 (indexed over all neurons) at
 219 frequency k and trial l is described as the product of network parameters, summed over networks F ,
 220 plus an error term $\varepsilon_{j_1 j_2 k l}$. The phase of the network-specific product is given by the difference in the
 221 time profiles ($\sigma_{j_1 f} - \sigma_{j_2 f}$) of neuron j_1 and j_2 multiplied by the frequency φ_k in Hz, multiplied by 2π . This
 222 phase is then weighted by the product of the two neurons' neuron profile $a_{j_1 f} \cdot a_{j_2 f}$, the (squared)
 223 frequency profile b^2 at frequency k , and the (squared) trial profile c^2 at trial l . As is observed here, the
 224 technique also produces a *frequency profile* per network, describing how important each frequency is
 225 for a network. For the purpose of spike timing networks, we will ignore this, as it does not provide
 226 additional information. It is, however, an essential element of its original application on
 227 electrophysiological recordings, describing frequency band-specific phase-coupled oscillatory networks,
 228 such as traveling waves.

229 Compared to the reference publications, the above equation squares the trial and frequency
 230 profile. The reason for this, is that spike timing networks are more conveniently thought of, analyzed at,
 231 and simulated in, the description level of cross spectra. This is not the case for the original target of the
 232 technique, phase-coupled oscillatory networks, which are more conveniently thought of as time-varying
 233 oscillations over electrodes described by Fourier coefficients (of which the cross products over time
 234 produce the cross spectra). Due to this, the technique provides trial and frequency profiles that are not
 235 squared, and squaring becomes a necessary step prior to investigating the extracted networks.

236 The extracted networks are unique up to trivial indeterminacies without requiring constraints
 237 such as orthogonality or statistical independence. Uniqueness is discussed in more detail in the
 238 reference publications (van der Meij et al., 2015, 2016). The indeterminacies are easily resolved by
 239 normalizations. Here, we briefly highlight those normalizations that pertain to the current application of
 240 the technique. The neuron and trial profiles, per network, have undetermined multiplicative scaling, and
 241 are normalized to have a vector L2-norm of 1. The consequence is that the absolute values of neurons
 242 and trials only have meaning with respect to the other neurons and trials of the same network. Crucially,
 243 the ratios between neurons and trials are unaffected by this normalization, and can be compared freely
 244 across networks. Additionally, their sign is also undetermined, and restricted to have a positive average
 245 per network (neuron profile) or to be fully positive (trial profile). The indeterminacy of the time profile is
 246 more complicated. Because the time profile describes circular phases over multiple frequencies, the
 247 time profile is circular as well. In short, we normalize it such that the strongest neuron (of the neuron
 248 profile) has a time profile value of 0s. Due to the above normalizations, a network-specific multiplicative
 249 scaling parameter is also extracted, but it does not play a role in the interpretation of the individual
 250 network parameters.

251 Two practical points need to be made for using the technique to extract networks. The first is
 252 that its algorithm is initialized from random starting values. In order to avoid unfortunate starting values
 253 that lead to a local minimum of its least squares loss function, the algorithm needs to be initialized
 254 multiple times. When identical networks are found in those initializations with the highest explained
 255 variance, it can be assumed that the global minimum is reached. How many initializations are required
 256 in order to achieve this depends on the particular dataset. In our experience, it is extremely rare to find
 257 a different 'best' solution to the loss function when increasing the number of random initializations
 258 beyond 50. The second practical point is that, like related decomposition techniques, the number of

259 networks to extract needs to be determined. One approach is to estimate the number of *reliable*
 260 networks. For this, we extract N networks from the full recording, and also from two splits of the
 261 recording, the first containing the odd numbered spikes of each neuron, the second the even numbered
 262 spikes. If the networks from the full recording reasonably match those extracted from of both splits, N is
 263 increased, and the process is repeated until they no longer match. The networks extracted from the full
 264 data are kept, and those of the splits discarded. Other scenarios are also feasible, such as an odd-even
 265 trial split, or a k -split approach, in which networks are extracted from k subsets of the recording and
 266 compared to those extracted from the full recording. The number of splits, and the manner of splitting,
 267 will determine the sensitivity of the approach. It is useful here to make a technical statement regarding
 268 the splitting of individual networks into two or more smaller networks, which would complicate the
 269 above. In order to avoid such splitting, network interaction terms in the decomposition model are forced
 270 to be zero (interaction terms are not visible in the element-wise model above; for optimization details
 271 see van der Meij et al., 2015, 2016). A practical consequence is that spike timing networks that are
 272 nearly perfectly correlated (share spike sequence timing) will likely be extracted as a single combined
 273 network (see van der Meij et al., 2016 for simulations investigating network correlation). Finally,
 274 regarding the maximum number of networks that can be uniquely extracted, though non-trivial to
 275 estimate (Comon et al., 2009), it likely is greater than the number of neurons. Importantly, any kind of
 276 reliability procedure such as the above will prevent exceeding any maximum, as non-unique networks
 277 will, by definition, not be reliable over splits. In our experience, the number of reliable networks is often
 278 much lower than the number of recorded neurons.

279 To determine whether two networks are similar, such as in the above split-reliability approach, a
 280 coefficient can be computed for the three parameters of the networks. For the neuron and the trial
 281 profiles, this is simply the inner product between the L2-normalized profiles of two networks, and
 282 ranges from 0 to 1 (identical profiles). For the time profile, a coefficient is the following:

283 *time profile similarity: $|(A^1 \cdot \exp(i2\pi\gamma\sigma^1), A^2 \cdot \overline{\exp(i2\pi\gamma\sigma^2)}|$*
 284 Time profile similarity is computed as the absolute value $|\cdot|$ of the inner-product $\langle \cdot, \cdot \rangle$ over neurons J
 285 of the time profiles σ of two networks (superscript 1 and 2, $\overline{\cdot}$ denotes complex conjugate), weighted by
 286 the normalized neuron profiles A of each network (\cdot denotes the element-wise product). Here, γ stands
 287 for the greatest common divisor of the frequencies used to extract the networks, in Hz, which
 288 determines the ‘cycle length’ of the circular time profile (van der Meij et al., 2015). This similarity
 289 coefficient also ranges from 0 to 1 (identical profiles). Allowing for some differences in the profiles due
 290 to noise, we considered networks similar enough when coefficients for the neuron, time, and trial,
 291 profiles are all equal to, or greater than, 0.7.

292 *Software and code accessibility*

293 The technique is freely available in a public GitHub repository termed *nwaydecomp*
 294 (www.github.com/roemervandermeij/nwaydecomp), together with tutorials on its use. The toolbox also
 295 contains software to deal with the practical points above. The code is also available as Extended Data 1.

296 **3. Obtaining cross spectra that are optimal for extracting spike timing networks**

297 To be able to extract spike timing networks we compute cross spectra from binary spike trains, by
 298 convolving the spike trains with complex exponentials (‘wavelets’) and computing their cross products
 299 over time (Fig 1, step 1-2). Doing so transforms the time delays between spikes of different neurons,
 300 into phase differences at multiple frequencies. The length of the complex exponentials, and their
 301 frequency, determines how sensitive the cross spectra are to consistent vs non-consistent time delays,
 302 and is described in the following. Here, it is important to keep in mind that the cross spectrum between
 303 two neurons, is *exactly* the complex-valued sum, of the phase differences between spikes of neuron 1
 304 and spikes of neuron 2 that are overlapping after the convolution, weighted by their amount of

307 temporal overlap. Due to the latter, long time delays necessarily have lower weighting in the cross
 308 spectra than short time delays.

309 Obtaining the cross spectra can be expressed as follows:

$$310 \quad X_{j_1 j_2 k l} = Z_{j_1 k l} Z_{j_2 k l}^* \\ 311 \quad Z_{j k l} = S_{j l} \otimes \exp(i T 2\pi \varphi_k)$$

312 That is, the cross spectrum between neuron neurons j_1 and j_2 at frequency k and trial l is obtained as
 313 the cross product, over time, of vectors $Z_{j_1 k l} Z_{j_2 k l}^*$ ($*$ = complex conjugate transpose). The vector $Z_{j k l}$ for
 314 neuron j is obtained by the convolution \otimes of the binary spike train vector $S_{j l}$ with a complex exponential
 315 (untapered ‘wavelet’, i is the imaginary unit) at frequency φ_k . Here, T is a vector of time points from
 316 $-t/2$ to $t/2$, with t being the time domain length of the complex exponential, and both $S_{j l}$ and T are
 317 sampled at the maximum achievable sampling rate. Note, the edges of $Z_{j k l}$, for which the complex
 318 exponential was not fully immersed in $S_{j l}$, are kept.

319 The time domain length t of the complex exponentials determines which between-spike time
 320 delays can contribute to the cross spectra, and it should be chosen based on the expected range of time
 321 delays. Here, we aim to be sensitive to time delays of 0 ± 10 ms, a range that captures commonly
 322 occurring consistent spike timing (e.g., Nelson et al., 1992; Fujisawa et al., 2008; Sakurai et al., 2013).
 323 The optimal time domain length for this range is a trade-off. The longer the length, the lower the
 324 sensitivity will be to the expected time delays, as the cross spectra will reflect a sum of more spike pairs.
 325 The shorter the length, the bigger the ratio between the weighting (samples overlap) of the shortest and
 326 the longest expected time delay, and thus the stronger the bias in sensitivity towards the former. As a
 327 compromise between the two, we choose a time domain length of twice of the maximum time delay we
 328 wish to be sensitive for, 20ms. This results in an overlap of 50% of the complex exponentials’ samples for
 329 spikes at a delay of ± 10 ms, having an acceptable sensitivity bias ratio of 0ms (shortest; 100% overlap)
 330 to ± 10 ms of 2:1 (compared to 400:1 for 0ms: ± 20 ms at a sampling rate of 20kHz). When there is no a
 331 priori expectation regarding the length of the time delays, the time domain length t can be based on,
 332 e.g., an investigating of the peak of the between-neuron cross correlograms. In general, it is preferable
 333 to choose a length t that is too long rather than too short, as the sensitivity cost due to additional spike
 334 pairs in the cross spectrum is much less than that of (1) a more skewed sensitivity bias ratio and (2) the
 335 experimental cost of spike time consistency at longer delays being invisible. In order to further reduce
 336 the bias of short time delays to long time delays, the complex exponentials should have constant
 337 magnitude, and not be tapered using a particular windowing function (such as a Hanning window).

338 The frequencies φ of the complex exponentials greatly determine the sensitivity of the cross
 339 spectra to non-consistent time delays. In order to be maximally sensitive to consistent time delays, the
 340 contribution to the cross spectrum of all other time delays should be as small as possible. In the terms of
 341 phase differences in the cross spectra, this is achieved when the average of the complex-valued phase
 342 differences of the non-consistent time delays approaches a magnitude of 0. This is the case for any
 343 frequency whose cycle length is an integer multiple of the time domain length chosen above (for 20ms,
 344 50Hz, 100Hz, 150Hz, etc.), under the assumption that non-consistent spike pairs are equally likely at any
 345 time delay. To arrive here, it is crucial to appreciate the fact that phase differences for large time delays
 346 are weighted lower than those for small time delays. For phase differences originating from time delays
 347 between 0ms and the time domain length (20ms above) to have an average magnitude of 0, the
 348 weighting coefficients for phase differences between $\pi/2$ to $-\pi/2$, the left side/quadrant 2 and 3 of the
 349 unit circle, need to have the same sum as those for $-\pi/2$ to $\pi/2$, the right side/quadrant 1 and 4 of the
 350 unit circle. Crucially, for the frequency whose cycle length equals the maximum time delay, the 25%
 351 smallest time delays fall in quadrant 1, the middle 50% of time delays fall in quadrant 2 and 3, and the
 352 25% largest time delays fall in quadrant 4. Equally crucial, the weighting is a linear function of the time
 353 delays. As for any linear function the sum of the first 25% and the last 25% of a subset of its values is
 354 equal to the sum of its middle 50%, the frequency with a cycle length equaling the largest time delay will

355 have phase differences from non-consistent time delays that approach an average magnitude of 0. This
 356 also holds for any integer multiple N of this frequency, as the above will be the case for N equal splits of
 357 the time delay range. Note that to obtain an average magnitude of 0, it is also required that the sum of
 358 weighting coefficients for quadrant 1 and 2 (top of unit circle) is equal to that of quadrant 3 and 4
 359 (bottom of unit circle). This symmetry is easily achieved however, as the weighting coefficients for -
 360 20ms to 0ms progress along the unit circle in opposite direction than those for +20ms to 0ms. As a last
 361 note, the frequencies of the complex exponentials also determine the robustness to jitter around a
 362 consistent time delay. The lower the frequency, the closer the phases of jittered but consistent time
 363 delays, the higher their average magnitude, and thus, the more robust to jitter.

364 Concluding, we compute cross spectra by convolving spike trains with complex exponentials of
 365 20ms length, constant magnitude, and at 20 frequencies from 50Hz to 1000Hz in steps of 50Hz. When
 366 investigating longer time-scale neuronal dynamics, an analogous set would be e.g. 1s length, at 1Hz to
 367 20Hz in steps of 1Hz. The number of frequencies to use is somewhat arbitrary. Initial simulations
 368 showed no noticeable difference beyond 20 frequencies (and 1000Hz is already very sensitive to jitter),
 369 and simulated networks were reliably recovered from simulations as little as 5 frequencies.

370

371 **4. Normalizations of the cross spectra**

372 The neuron profiles of spike timing networks describe the off-diagonal elements of each cross spectrum,
 373 reflecting between-neuron spike pairs, and the diagonal elements, i.e. power, reflecting the total
 374 number of spikes of neurons. In realistic data, the firing rates of neurons can differ greatly, resulting in
 375 large differences in power. Because the power of each cross spectrum is typically much larger than its
 376 off-diagonal elements, this can lead to spike timing networks whose neuron profiles are driven more by
 377 firing rates of individual neurons, rather than consistent spike timing between neurons. An extreme
 378 example is a neuron profile with a non-zero weighting for only a single neuron. Such a 'network' only
 379 describes the diagonal element (i.e. firing rate) of the cross spectra of the respective neuron, and should
 380 be considered as an artefactual network. To increase sensitivity to consistent spike timing, in order to
 381 avoid the above, power differences between neurons can be normalized (Fig 1, step 3). Normalizing
 382 power such that it is equal to an Nth root, summed over frequencies and trials, is one such
 383 normalization:

$$384 \quad X_{kl} = W^{\frac{1}{N}} X_{kl} W^{\frac{1}{N}}$$

neuron-wise normalization:
$$W = \frac{\sum_K \sum_L [X_{kl}^{diag}]^{\frac{1}{N}}}{\sum_K \sum_L [X_{kl}^{diag}]}$$

385 Here, X^{diag} is a diagonal matrix containing only the diagonal elements of X . By increasing N, the power
 386 differences between neurons decrease. Ideally, the power of every neuron becomes equal, i.e. the cross
 387 spectra become coherency spectra, as this will have the highest sensitivity to spike time consistency.
 388 However, this can have the unintended consequence of interfering with the split reliability procedure
 389 for estimating how many networks to extract. Briefly, when extracting fewer than the total number of
 390 networks, which networks are extracted strongly depends on their explained variance; those with the
 391 most, tend to be extracted first (as the networks are found by a randomly initialized least squares
 392 algorithm). When the differences in explained variance between networks decrease, the order in which
 393 they are extracted becomes more variable, which can prematurely stop the split reliability procedure.
 394 Increasing neuron-wise normalization strength can result in decreasing differences in explained
 395 variance. As such, while neuron-wise normalization increases the usefulness of the networks, it can also
 396 result in finding less split-reliable networks. Practically, an optimal normalization strength can be found
 397 as follows. First, a split reliability procedure is run with normalization strength N = 1 (no normalization).
 398 If this results in, (1) split-reliable networks, and, (2) networks that are unlikely to reflect spike time
 399 consistency (neuron profiles that have strong weighting for only one neuron), the normalization

400 strength N is doubled and the split reliability procedure repeated. This is repeated until sufficient
 401 reliable networks are found that reflect spike consistency. A convenient quantification of when
 402 networks are unlikely to reflect spike time consistency is to compute the ratio of the strongest and
 403 second strongest weights of the neuron profile; the higher this ratio, the more likely the second
 404 strongest weight reflects noise and that the network does not reflect spike time consistency. Then, in
 405 the above procedure, a cut-off ratio of 5-to-1 can be used as a conservative criterion (see also Results
 406 section 5). Crucially, the above only affects the probability of uncovering those spike timing networks
 407 that already exist in the recording, the phase coupling structure in the cross spectra induced by the
 408 networks remains unaffected.

409 The firing rate of neurons can also differ greatly between trials. Because the trial profile reflects
 410 variations in the cross spectra over trials in its weights, it reflects both the trial-specific firing rate of the
 411 involved neurons as well as their trial-specific amount of spike timing consistency. Similar to the above,
 412 normalizing the cross spectra over trials can reduce the impact of firing rate on the trial profile.
 413 Normalizing cross spectral power such that it is equal across trials is one such normalization:

$$414 \quad \begin{aligned} X_{kl} &= W_{kl}^{\frac{1}{2}} X_{kl} W_{kl}^{\frac{1}{2}} \\ \text{trial-wise normalization:} \quad W_{kl} &= \frac{1}{\sum_L X_{kl}^{diag}} \sum_L X_{kl}^{diag} \end{aligned}$$

415 As above, X^{diag} is a diagonal matrix containing only the diagonal elements of X . Importantly, in the
 416 common case of a neuron not spiking in a particular trial, its elements of the cross spectra (X) will be
 417 zero, leading to division-by-zero errors during the above normalization. This is avoided by adding
 418 random noise of trivial strength (close to the used numerical precision) to the respective elements of the
 419 cross spectra prior to normalization. Trial-wise normalization is achieved by first normalizing frequency-
 420 and trial-specific cross spectral power to 1 (by division by itself), and then multiplying it with the
 421 frequency-specific summed power over trials ($\sum_L X_{kl}^{diag}$; computed prior to normalization). Trial-wise
 422 normalization is independent of the above neuron-wise normalization, both normalizations can be
 423 applied jointly. The normalization above is extreme, as it removes all cross spectral power variability
 424 over trials. However, because normalization occurs via a diagonal matrix (as is the case with neuron-
 425 wise normalization), the off-diagonal elements of the cross spectra only undergo a scaling proportional
 426 to their diagonal elements; their magnitudes still reflect the (relative) amount of spike timing
 427 consistency between their involved neurons. As such, the remaining trial-by-trial variations in cross
 428 spectral magnitudes maximally reflects trial-by-trial variations in the amount of spike timing consistency.
 429 Similar to the neuron-wise normalization, the trial-wise normalization can make it harder to uncover
 430 networks that are present in the recording. This can be dealt with more conveniently however. First,
 431 networks are extracted using a split reliability procedure as discussed above, without trial-normalizing
 432 cross spectra. Once reliable networks are obtained, the trial profiles are re-estimated in one final
 433 decomposition using cross spectra that are additionally trial-normalized, in which the neuron and time
 434 profiles are kept constant. Although the above 2-step approach is advised, in the case of our simulations
 435 the differences were negligible, and for simplicity the results that are presented were extracted from
 436 trial-wise normalized cross spectra in one step.

437

438 5. Simulating and extracting noisy spike timing networks

439 To investigate the effects of various kinds of noise on spike timing network extraction, we simulated
 440 spike recordings of 15 neurons at 100 trials of 1s containing 4 spike timing networks. Network spiking
 441 sequences had a fixed temporal structure that was repeated between 0-3x (predetermined) per trial
 442 (1.2Hz average spike sequence rate for each network). Within each trial, each spike sequence could
 443 occur anywhere with uniform probability, with a 25ms offset from trial boundaries. On trials where
 444 spike sequences of multiple networks were present their order was randomized, and with a minimum of

445 25ms between sequences. Three kinds of noise were simulated. First, all neurons of a single simulation
 446 had a noise spiking rate of 0Hz, 5Hz, 10Hz, 20Hz, or 100Hz, as Poisson spiking superimposed on the
 447 network spike sequences. Second, each spike of each spike sequence could have an individual random
 448 jitter (uniformly distributed) at a maximum of 0ms, ± 0.25 ms, ± 0.5 ms, ± 1 ms, or ± 2 ms. Third, each spike
 449 in each spike sequence occurrence had an individual deletion probability of 0%, 10%, 20%, 40%, 80%,
 450 resulting in partial spike sequences. Cross spectra of each simulation run were obtained as described
 451 above, using a time-window length of 20ms and frequencies from 50Hz to 1000Hz in steps of 50Hz. The
 452 4 networks were extracted using 10 random initializations of the extraction algorithm. Note that the
 453 purpose of these simulations is to show how well spike sequences can be extracted under noisy
 454 conditions, and not how such a pattern can be generated physiologically, nor whether such a pattern is
 455 physiologically meaningful. As such, we simulated data from the perspective of spikes, instead of model
 456 neurons generating spikes, which also provides a convenient ground truth for calculating recovery.
 457

458 6. Quantifying recovery of simulated spike timing networks

459 To quantify the recovery of the extracted neuron profile, time profile, and the trial profile, they were
 460 compared to their simulated equivalents. The simulated neuron profiles were constructed as a binary
 461 $1 \times J$ vector per network, its values indicating network membership of each neuron. Similarly, simulated
 462 trial profiles were constructed as $1 \times L$ vector, its values reflecting the number of sequence repeats
 463 (linear modulation of network activity over trials). Finally, simulated time profiles were constructed as a
 464 $1 \times J$ vector, its values describing the temporal sequence of spikes in seconds (non-member neurons set
 465 arbitrarily to 0). For display purposes these simulated parameters were normalized in the same manner
 466 as the extracted network parameters. In order to compute recovery, extracted networks were paired to
 467 the simulated networks using the similarity coefficients described above, by first determining the most
 468 similar pair, then the next most similar in the remainder, etc. Recovery of neuron and trial profiles was
 469 determined using a Pearson correlation coefficient. Time profile recovery was judged by the following
 470 coefficient:

$$471 \text{time profile recovery: } \frac{|\sum_j \exp(i2\pi\gamma\sigma^e) \cdot \overline{\exp(i2\pi\gamma\sigma^s) \cdot A^s}|}{\sum_j A^s}$$

472 Time profile recovery is computed as the absolute value $|\cdot|$ of the weighted sum over neurons J of the
 473 complex-valued difference of the circular time profiles σ of the extracted and simulated networks
 474 (superscript e and s resp.; $\overline{\cdot}$ denotes complex conjugate), weighted by the simulated neuron profile A (\cdot
 475 denotes the element-wise product). Similar to the similarity coefficient described above, γ is the
 476 greatest common divisor of the frequencies used for extraction (i.e., 50Hz), and is used to deal with the
 477 circularity of the time profile. This coefficient ranges from 0 to 1 (perfect recovery).
 478

479 7. Extracting spike timing networks from recordings of rat medial prefrontal cortex and hippocampus

480 As a proof of principle, we extracted spike timing networks from real spiking recordings, obtained from a
 481 dataset publicly available at CRCNS.org (Fujisawa et al., 2008, 2014). This dataset contains identified
 482 neurons and their spikes from recordings obtained from rat medial prefrontal cortex and area CA1 of
 483 the hippocampus, while the rat performed an odor-based delayed matching-to-sample task, requiring it
 484 to run through either the left or right arm of a maze to obtain its reward. Animal recording protocols
 485 were approved by the Institutional Animal Care and Use Committee of Rutgers University, Newark, NJ,
 486 USA. The recording used (rat GG.069) came from 8 and 4 electrode shanks (200 μ m shank separation) in
 487 medial prefrontal cortex and CA1 respectively, each shank containing 8 contacts (20 μ m contact
 488 separation; 160 μ m² contact surface). The recording was sampled at 20kHz, and offline spike sorting was
 489 performed (after band-passing between 0.5-5kHz) using KlustaKwik (for spike sorting details see
 490 Fujisawa et al., 2008, 2014). 63 neurons were identified on 9 shanks. The dataset contained 20 left and
 491 20 right trials, having an average duration of 8.04s (SD = 1.73s). Only neurons with average spiking rates

492 of 1Hz and above were selected. In order to extract networks, we first obtained cross spectra as
493 described in Materials and Methods section 3, using a time window of 20ms and frequencies from 50Hz
494 to 1000Hz in steps of 50Hz, dividing each cross spectra by its trials' duration. Subsequently, cross spectra
495 were neuron-wise normalized as described above. A normalization such that cross spectral power was
496 equal to its 32nd root normalization was chosen as an optimal normalization, because 64th root
497 normalization resulted in no split reliable networks (likely due to varying network order mentioned in in
498 Materials and Methods section 4), and 16th root normalization resulted in many networks mostly
499 consisting of single neurons (i.e. the bias towards power differences between neurons was too strong to
500 overcome). The number of networks to extract was determined using odd-even spike split reliability
501 procedure described in Materials and Methods section 2 with a similarity coefficient cut-off of 0.7, 50
502 random initializations were used at each step. This resulted in 4 networks being extracted. Continuous
503 cross-correlograms were obtained at time lags of ± 20 ms at 0.05ms steps by summation of the (lagged)
504 binary spike trains after they were convolved with a Gaussian with full-width at half-maximum of 0.5ms
505 (maximum = 1).
506

507 **Results**

508

509 Spike timing networks consist of multiple neurons that have consistent time delays between their
510 spikes, forming a spike sequence. Here, we validate a novel approach for finding and characterizing
511 these networks in neuronal spike recordings. First, we evaluate its robustness to various noise
512 conditions. We show how the recovery of simulated spike timing networks is affected by spike jitter in
513 the network spike sequences and variability of neuron participation in the network, under increasing
514 spiking noise of all simulated neurons. Then, we show how variable firing rates of neurons affects
515 recovery, and what actions can be taken to reduce negative effects. Finally, we provide a proof-of-
516 principle by showing networks extracted from rat hippocampus and medial prefrontal cortex (Fujisawa
517 et al., 2008, 2014), and compare the extracted spike timing relations to cross-correlograms of the
518 involved neurons.

519

520 1. Simulated spike recordings from spike timing networks

521 To investigate the robustness of spike-timing network extraction to various kinds of noise we simulated
522 spike recordings of 15 neurons over 100 trials of 1s containing 4 networks (for simulation details see
523 Materials and Methods section 5). A network was defined as a group of neurons that spike in sequence,
524 with between-spike time delays ranging from 0 (synchronous) to 2.5ms. The spike sequence timelines
525 were 0-0-1-1.5-2.5-3-4.5-6.5ms for network 1, 0-1-2-3-4ms for network 2, 0-0-0-0ms for network 3 (all
526 synchronous), and 0-2.5-7.5ms for network 4. Each network's spike sequence was repeated 0-3 times in
527 groups of trials to simulate linear modulations of network activity across the task. Some of the networks
528 had neurons that were involved in other networks' spike sequences: all of the neurons of the spike
529 sequence of network 2 were also part of network 1, and one neuron was shared between network 1 and
530 3, and network 3 and 4. In Figure 2A-C we show the networks' *neuron profiles* (Fig 2A), *time profiles* (Fig
531 2B), and *trial profiles* (Fig 2C). The simulated recordings of the 15 neurons result in many pair-wise spike
532 time relationships between neurons, which we show schematically in Figure 2D. These pair-wise
533 relationships can also be visualized as cross-correlograms for all neurons, which we show in Figure 2E.

534 The profiles in Figure 2A-C are directly comparable to the three profiles of spike timing networks
535 extracted using our approach (see Materials and Methods section 1 for how to interpret the profiles),
536 and are used in Results sections 2-4 for judging recovery of the simulated networks by the extracted
537 spike timing networks. Note, the absolute values of the neuron and trial profiles are not meaningful,
538 only the *within-network ratios* are (see Materials and Methods section 2). As such, it is not the spike
539 sequence repeats per trial that is described by the trial profile (i.e. 0, 1, 2, 3; Fig 2C), but rather the ratio
540 between them (e.g. a trial with 3 sequences having a weight 3x that of a 1 sequence trial).

541 To investigate when the recovery of the simulated networks fails, we varied the strength of
542 three kinds of noise (see Materials and Methods section 5). These were: (1) spiking noise, or non-
543 network spikes, superimposed on the spike sequences (see Fig 2F), (2) jitter of each spike in a spike
544 sequence occurrence, and, (3) partiality of network spike sequences (random spikes missing from the
545 sequence). The range of each of the noise levels was chosen to provide an intuition for when an
546 expected network can still be recovered, and to progressively result in failure to recover the simulated
547 networks. As such, the higher levels are not necessarily physiologically reasonable. The simulated
548 networks were also different in size, spike sequence timing, spatial overlap, and trial overlap, to increase
549 the likelihood that any related weaknesses of the technique would be revealed.

550

551 2. Recovery of simulated spike timing networks with spiking jitter when surrounded by spiking noise

552 Neurons can be noisy, and any spike sequence of a spike timing network is likely embedded in other
553 spikes of the same neurons. Furthermore, precise spike times depend on the fluctuating membrane
554 potential of the neuron and other factors, potentially adding temporal jitter. To investigate how these

555 two factors influence network characterization, we simulated spike timing networks with different levels
556 of background spiking noise and with different levels of jitter of each spike in the spike sequences.
557 Networks were simulated 50 times for each combination of the noise factors. We computed recovery of
558 simulated networks and show the result in Figure 3. Recovery of the neuron and trial profiles was
559 computed as the Pearson correlation between the recovered and simulated profiles. For the trial
560 profiles, the correlation also directly reflects the recovery of the linear modulation of network activity
561 across the task (perfect recovery is 1). Recovery of the time profiles was computed using a recovery
562 coefficient that ranges from 0 to 1 (perfect recovery; see Materials and Methods section 2).

563 Firstly, we observe that with reasonable jitter (i.e. ± 0.25 ms compared to 0-2.5ms spike
564 sequence delays) and spiking noise (e.g. 20Hz vs 1.2Hz average network spiking rate) the neuron and
565 time profiles were recovered with reasonable accuracy, with the trial profile being the most affected. At
566 20Hz spiking noise and ± 0.25 ms jitter the linear modulation of network activity was still visible but
567 weakened (Fig 3, bottom: mean (SEM) over simulations of Pearson's correlations for network 1-4: 0.78
568 (0.02), 0.29 (0.02), 0.62 (0.01), 0.44 (0.01)). Shown in the examples (Fig 3, bottom), the effect of noise on
569 the trial profile can be observed as a shrinking of the ratios between loadings of trials with a different
570 number of simulated network sequences and an increase in the trial profiles 'baseline'; the loadings of
571 those trials which had 0 network sequences. The latter is important in practice, because under the
572 assumption that a network is not active in all trials, the lowest trial loadings with respect to the higher
573 trial loadings can be used as an indication of the reliability of network parameters. Secondly, we observe
574 that, except from the largest jitter case (± 2 ms), network spike jitter had a similar effect on recovery of
575 network parameters as spiking noise, as evidenced by the similarity between the 10Hz/0ms and the
576 5Hz/ ± 0.25 ms cases, and the 20Hz/0ms and the 5Hz/ ± 0.5 ms cases. Thirdly, we observe that, under
577 strong noise conditions (>20Hz spiking noise and $> \pm 1$ ms jitter), the linear modulation of network activity
578 became very weak to largely invisible (maximum mean Pearson's correlation over simulations of 0.11,
579 0.04, 0.23, 0.08 for network 1-4). Regarding network specific recovery, though there was some variation
580 in recovery, apart from the above, the differences were minimal and did not highlight a sensitivity to a
581 particular aspect of the simulated networks.

582

583 **3. Recovery of simulated spike timing networks with partial spiking when surrounded by spiking 584 noise**

585 To investigate how partial spiking in spike timing networks, i.e. not all member neurons joining in each
586 spike sequence, affects characterization of the full spike sequences, we simulated networks where each
587 spike of a sequence had a chance to be deleted. Similar to the above, we did so 50 times for each level
588 of spike deletion probability, and of spiking noise. The results are shown in Figure 4. We observe that,
589 (1) as the chance of spike deletion increased, recovery accuracy was decreased, (2) as with spiking
590 jitter/noise, the trial profile was more affected by noise than the neuron profile, (3) as with spiking
591 jitter/noise, the effects of spike deletion on recovery were similar to those of spiking noise, (4) the full
592 spike sequences in the time profile were accurately extracted under reasonable noise (20Hz) with 40%
593 probability of spike deletion, even though the majority of individual spike sequences were incomplete,
594 and, (5) under the same noise conditions the linear modulation of network activity was weak but
595 detectable for networks 1 and 3, and nearly invisible for networks 2 and 4 (mean (SEM) Pearson's
596 correlation over simulations of 0.39 (0.02), 0.06 (0.02), 0.29 (0.02), 0.08 (0.02) for networks 1-4). These
597 differences possibly stem from network overlap (network 2 shares all its neurons with network 1) and
598 network size (network 3 is the smallest).

599

600 **4. Cross spectra normalization diminishes effects of differential firing rates of units and trials**

601 The spike timing networks simulated above were extracted under noise related firing rates that were
602 identical over neurons and over trials. This was chosen to show the overall effect of spiking noise, but is

603 atypical for real recordings. Here, we show the effect on network recovery of firing rate differences
604 between neurons and trials, while keeping the number of spike sequences constant.

605 We first show the recovery of simulated networks when the firing rate differs over neurons (Fig
606 5). We simulated networks 50 times, with neuron 5 (a member in network 1 and 2) and neuron 12
607 (member in network 3 and 4) having 100Hz spiking noise, the other neurons 5Hz (Fig 5A). Network
608 spiking jitter was ± 0.25 ms. The recovery of the networks (Fig 5B; compare to Fig 2) was distorted: (1) the
609 neuron profiles of the networks for neurons 5 and 12 were strongly increased/decreased, (2) the noise
610 of neuron 5 led to a strong loading for network 3, of which it was not a member, (3) network 4 was
611 dominated by neuron 12, (4), the trial profiles showed decreased recovery (compared to Fig 2), and (5)
612 although the time profile of networks 1, 2, and 4 were not (noticeably) distorted, network 3's is. Overall,
613 the differential firing rate can be said to have pulled the estimated network parameters towards those
614 neurons with more spiking. This effect however, can be substantially reduced by normalizing cross
615 spectra prior to network extraction. Here, we show the effect of normalizing cross spectra such their
616 power is equal to their N th root (see Materials and Methods section 4), reducing differences in firing
617 rates. We show its effects progressively by using $N = 2, 4, 8, 16, 32$ (Fig 5C), and ending with $N = 64$ (Fig
618 5D). We observe that (1) the recovery of the neuron profiles was improved, with network 1 showing the
619 most remaining distortion at neuron 5, (2) the trial profiles were similar to the case with 5Hz spiking
620 noise for all neurons (see Fig 2), and, (3) the recovery of the time profile of network 3 was improved
621 such that the distortion is minimal.

622 To investigate the effect of differential spiking rate over trials we simulated networks with 5Hz
623 spiking noise, except for trials 21 to 60, which had 10Hz spiking noise (Fig 6A). Network spiking jitter was
624 set at ± 0.25 ms spiking jitter, and networks were simulated 50 times. The trials with additional spiking
625 noise were chosen such that they both involved 100% of trials of sequence repeats (1x and 2x for
626 network 1, 1x for network 2, 1x for network 4) and a partial set of sequence repeats (50% of 1x and 2x
627 for network 3, 50% of 0x for network 2). The recovery without normalization is shown in Figure 6B. We
628 observe that (1) the recovery of the neuron profiles and time profiles was similar to the case of 5Hz
629 noise and ± 0.25 ms spiking jitter (see Fig 2) and, as such, they were minimally affected by the differential
630 noise over trials, (2), the linear modulation of network activity was recoverable, but weakened, for all
631 networks (especially network 3; mean (SEM) Pearson's correlation over simulations of 0.93 (<0.01), 0.67
632 (0.01), 0.76 (<0.01), 0.36 (0.01) for network 1-4) compared to without trial variations of firing rate (0.98
633 (<0.01), 0.94 (<0.01), 0.89 (<0.01), 0.77 (0.01); Fig 3), and, (3) the trial profile loadings for those trials
634 affected by increased spiking noise were distorted such that the ratios of loadings no longer reflected
635 the correct order of the number of sequence repeats (i.e. 1x>2x trials for network 2 and 4). Though the
636 linear modulation was moderately recoverable, the latter means an investigation of the network
637 activities in specific trials of network 2 and 4 (supported by e.g., an independent samples t-test) would
638 have resulted in the incorrect conclusion of more network activity being present in 1x compared to 2x
639 trials. As was the case for differential noise over neurons, normalization of the affected dimension can
640 improve recovery. Here, we normalized the cross spectra such that their power for every trial is equal to
641 their power summed over trials (see Materials and Methods section 4). Crucially, this does not affect the
642 ratio of the off-diagonal elements to the diagonal (power). As such, trials that have many spike
643 sequences (strong off-diagonal elements compared to power) are still distinguishable from trials with
644 few spike sequences (weak off-diagonal elements compared to power). Note, as well, that this trial-wise
645 normalization is unrelated to the neuron-wise normalization in the above, and they can be applied
646 jointly. We show the result of the trial-wise normalization in Figure 6C. We observe that, (1) the trial
647 profile recovery was improved such that the order of their loadings again reflected the order of the
648 number of sequence repeats, (2), recovery of the linear modulation of network activity was greatly
649 improved (mean (SEM) Pearson's correlation over simulations of 0.96 (<0.01), 0.96 (<0.01), 0.82 (<0.01),
650 0.89 (<0.01)), and, (3) though improved, the trial profiles' recovery was poorer than those at equal noise

651 levels for all trials (see Fig 3). We additionally observe that the normalization also affected the trial
652 profile loadings of trials that did not have increased noise. This was most noticeable in the loadings for
653 those trials of network 4 that had 0 and 2 sequence repeats (trials 1 to 20 and 61 to 100): the ratio of
654 the loading of 0 repeats to that of 2 repeats was much higher without normalization (Fig 6B), than with
655 normalization (Fig 6C). As trials with 0 repeats should ideally have a loading of 0, the higher this ratio the
656 better. Interestingly, even though the trial profile showed worse recovery overall, the recovery of the
657 linear modulation of network activity after trial-wise normalization was better than the recovery at
658 equal noise levels across trials without normalization, especially for network 4 (mean (SEM) correlation
659 of 0.89 (<0.01) and 0.77 (0.01) resp.). This was likely caused by the trial profiles of the former showing
660 less variability than those of the latter (i.e., the coefficient of variation of the trial profile of network 4,
661 averaged over simulations, was 14.1% and 27.9% resp.).
662

663 **5. Spike timing networks extracted from real recordings reflect between-neuron spike timing 664 relationships**

665 To provide a proof-of-principle we extracted spike timing networks extracted from spike recordings from
666 medial prefrontal cortex and hippocampus of a rat performing an odor-based delayed matching-to-
667 sample task (Fig 7; see Materials and Methods section 7). After odor presentation, the rat had to run
668 through the left or right arm of a figure-eight T-maze to obtain its reward. Networks were extracted
669 similarly to the simulations above, using a neuron-wise 32nd root power normalization, and a split-half
670 reliability approach to determine the number of networks (see Materials and Methods section 2). This
671 resulted in 4 extracted networks.

672 We show neuron profiles, time profiles, and trial profiles for each extracted spike timing
673 network in Figure 7. To provide a ground-truth estimate of whether the between-neuron spike times
674 from the networks reflect real spike timing relationships in the recordings, we also show for each
675 network continuous cross-correlograms (computed post-hoc; see Materials and Methods section 7) of
676 the neurons mostly strongly contributing to each network. Importantly, in each of these cross-
677 correlograms we indicate when the cross-correlation is expected to be highest, based on the time profile
678 of the networks.

679 For network 1, neuron pairs 1-2, 1-3, and 2-3 had peaks in their cross-correlograms that
680 matched the time profile's spike timing relationships within 0.03ms, 0.03ms, and 0.06ms respectively.
681 Neuron 4 does not appear to have consistent spike timing relationship with the first three, which is
682 unsurprising given that its weight in the neuron profile is much weaker (suggesting its weight reflects, at
683 least mostly, noise). Although there appears to be a difference in network activity between left and right
684 trials, this likely due to firing rate differences between conditions, as trial profiles calculated on trial-wise
685 normalized cross spectra showed no statistically significant difference (see Materials and Methods
686 section 4; this should be interpreted with caution however, as the profile's lowest weights suggested
687 they remained noisy). For network 2, neuron pairs 1-2, 1-3, and 1-4 had cross-correlogram peaks that
688 matched the time profile within 0.09ms, 0.07ms, and 0.19ms respectively. Neuron pair 2-3 and pair 3-4
689 did not have single cross-correlogram peak (though their center peaks matched within 0.17ms and
690 0.12ms resp.), and neuron pair 2-4 appears inhibitory. These observations could indicate that the spike
691 sequence did not involve all 4 neurons in a subset of trials. It is useful to reiterate here, that the
692 extracted spike sequence should be considered only at the level of the full recording (i.e. cross spectra
693 of all trials). That is, the extracted spike sequence should be considered as a description of the N-way
694 relationship between N neurons, i.e. the largest possible spike sequence for the network, and serve as a
695 starting point for targeted analyses. Network 3 show a similar pattern as network 1 and 2 according the
696 cross-correlograms, with the peaks of neuron pairs 1-2, 1-3, 1-4, and 2-3, matching the time profile
697 within 0.10ms, 0.09ms, 0.05ms, and 0.19ms resp. Network 4 likely reflects consistent spike timing only

698 between the strongest two neurons (matching within 0.08ms), as the neuron profile has few neurons
699 with strong loadings.

700 **Discussion**

701
702 Identifying and investigating cell-assemblies with spike timing consistency between neurons is key to
703 gain a further understanding of their role in neuronal coding (Bienenstock, 1995; Singer, 1999; Tiesinga
704 et al., 2008; Panzeri et al., 2010), but finding them is a tremendous challenge due to the possible
705 complexity of patterns of between-neuron spike time delays. Here, we introduced and validated, in
706 simulated and real data, a novel approach for extracting networks defined by their between-neuron
707 spike timing consistency, when forming sequences of time-shifted spikes, from neuronal spike
708 recordings (for other types of interactions, see e.g. Lindemann et al., 2001). The key features of this
709 approach are that (1) networks and their spike sequences can be extracted regardless of their
710 complexity in size and spike timing patterns, and (2) the spike sequences of the networks are specified
711 with high temporal precision. Networks consist of three profiles, describing (1) which neurons are
712 involved in which networks, (2) with which spike timing pattern, (3) in which trials or conditions. The
713 latter can in principle be used as an index for network activity. Together, these profiles form a
714 parsimonious description of the spike timing patterns in the recording, and can be used as a basis for
715 subsequent spike train analyses of experimentally relevant variations in network subsets. Using
716 simulations, we showed how the extracted networks were affected by spiking jitter, variability in
717 network participation by its member neurons, and non-network related spiking activity. Networks were
718 recoverable under reasonable noise conditions, with the time profile being especially robust to the
719 simulated noise. Though the trial profiles were strongly influenced by noise, they still tracked simulated
720 network activity to a degree. Using neuronal spike recordings from rats, we showed we were able to
721 extract networks from real recordings, of which the time profile reflected between-neuron spike timing
722 consistency that matched cross-correlograms with high accuracy. Together, this shows that our
723 approach can be useful for the investigation of spike timing networks.

724 The extracted networks can be of arbitrary complexity in size and time delays. This is a
725 consequence of the fact that the underlying method finds networks not in the *neuron-by-time* time
726 series, but in the *neuron-by-neuron* cross spectra. These cross spectra contain all of the spike timing
727 consistencies of the spike sequences, condensed into between-neuron phase coupling. Networks can be
728 separated when their spike sequences have different between-neuron phase coupling patterns, and
729 differences in phase coupling patterns over trials (or epochs) increases their separability. Networks are
730 extracted by finding those neuron, time, and trial profiles whose phase coupling patterns explain the
731 most variance in the cross spectra. Because the estimated profiles have the same size for each network,
732 larger networks only differ from smaller networks by their different distribution of weight magnitudes.
733 As a larger network does not involve estimating a larger number of weights, there is no combinatorial
734 explosion with increasing network size. In fact, higher complexity networks are likely easier to find than
735 lower complexity networks, as they will typically explain more variance in the cross spectra. The above is
736 different from techniques that search for template spike sequences in their original neuron-by-time
737 representations (Abeles and Gerstein, 1988; Nadasdy et al., 1999; Tetko and Villa, 2001; Lee and Wilson,
738 2002; Schnitzer and Meister, 2003; Ikegaya et al., 2004; Gansel and Singer, 2012). As these search for
739 exact spiking templates, they have to do so within some restricted space to avoid a combinatorial
740 explosion. Although finding high complexity networks is impractical with such approaches, they have the
741 advantage of being able to find spike sequences that repeat very few times in the course of a recording.
742 Because our approach is most sensitive to those networks that explain the most variance in the cross
743 spectra, it is not well suited for finding sequences with very few repeats, as they typically explain very
744 little variance in the cross spectra. As such, our approach trades sensitivity to such sequences for
745 sensitivity to sequences with arbitrarily high complexity, but that are more prominent.

746 An important aspect of the method behind our approach is that it is a decomposition of
747 between-neuron cross spectra over frequencies and trials into sets of network profiles. Because this

748 decomposition attempts to find profiles that parsimoniously explain all of the variance in the cross
749 spectra, its profiles need to not only describe between-neuron spike pairs, but also their total number of
750 spikes. Importantly, the latter typically outnumber the former to a strong degree (e.g., Gochin et al.,
751 1991; Nelson et al., 1992; Kreiter and Singer, 1996; Brosch and Schreiner, 1999). This impacts the
752 interpretation of the neuron profile weights. For any two neurons, their weights in the neuron profile
753 need to describe four magnitudes of the cross spectra: their total number of spikes in the magnitude of
754 their cross spectral power, and their spike timing consistency in the magnitude of their off-diagonal
755 elements. In the case these magnitudes differ, the neuron profile weights become a compromise, and
756 are drawn to those magnitudes that explain the most variance. These weights should therefore be
757 interpreted with caution, and should be considered more as an indication of network membership when
758 sufficiently away from 0, than as a straightforward index into the strength of their spike timing
759 consistency. This is also the reason why a neuron-wise normalization of the cross spectra is advisable, as
760 it will reduce the effect of firing rate differences. In fact, in our experience, when the cross spectra are
761 not neuron-wise normalized, few extracted networks will consist of more than one neuron (i.e.,
762 artefactual networks that are not based on spike timing). If it is also the case that the total number of
763 spikes of neurons differs more over trials than the number of their spike pairs do, then the trial profile
764 weights will be drawn towards the former, as they will explain more variance in the cross spectra. This
765 was likely the case for the networks we extracted from rat hippocampus and medial prefrontal cortex
766 (see e.g. network 1 in Fig 7), and is also likely the reason why the trial profile was strongly impacted by
767 simulated spiking noise. A trial-wise normalization for this was introduced, that in the specific case of
768 our simulations, improved recovery of the linear modulation of network activity. Nonetheless, the trial
769 profile remained sensitive to noise and, as such, should be used with caution, ideally with
770 complementary analyses (such as a targeted search, see below). The above contrasts with a previous
771 application on human electrophysiological recordings, where the trial profile was less sensitive to noise
772 (likely caused by more spatially extended networks; van der Meij et al., 2015, 2016).

773 Our approach describes the structure of spike timing consistencies in the cross spectra of the
774 entire recording. This means that the spike sequences represented by each network's time profile
775 describe the spike timing consistencies of the involved neurons over the entire recording. As such, the
776 time profile reflects an aggregate spike sequence, one that does not necessarily exactly repeat in each of
777 the involved trials. For example, some trials might only contain a part of the sequence. This property can
778 also be considered beneficial, and it is something we explicitly tested in our simulations with partial
779 spike sequences. In the case of strong variability in the exact spike sequence of every trial, the 'main'
780 sequence could still be identified.

781 The aggregate nature of our spike sequences contrasts with those of approaches that search for
782 exactly repeating spike sequences (Abeles and Gerstein, 1988; Nadasdy et al., 1999; Tetko and Villa,
783 2001; Lee and Wilson, 2002; Schnitzer and Meister, 2003; Ikegaya et al., 2004; Gansel and Singer, 2012).
784 These approaches typically also incorporate some form of statistical testing of the identified spike
785 sequences, which is necessary to obtain more certainty that the found sequences are not an accidental
786 consequence of statistical properties of the firing rates (see e.g. Grün, 2009, for a discussion of surrogate
787 data for this purpose). Importantly, we consider our approach not as an alternative to the above, but as
788 complementary. That is, our spike timing network profiles can be used to construct a network-specific
789 spiking template with between-spike time delays at high temporal resolution, that can be used in
790 approaches like the above to locate discrete occurrences of the network's spike sequences. This would
791 allow for subsequent investigations into, e.g., spike time variability within sequences, variable
792 occurrence of sequences over conditions, and spike sequence completeness, of network spike
793 sequences with a complexity that would otherwise be prohibitive.

794 Arguably the approaches closest to ours are those that also depend on neuron-by-neuron
795 representations to investigate spike timing consistency. Of these approaches, some start from a

796 Principal Component Analysis (PCA) on the between-neuron cross-correlations (Chapin and Nicolelis,
797 1999; Peyrache et al., 2010; Lopes-dos-Santos et al., 2011). These approaches result in a neuron profile
798 per component, describing correlated and anti-correlated neurons, and a temporal profile, providing a
799 component activity time course of some form that can be matched to the original neuronal spiking time
800 series. The biggest difference to our approach, is that, in those methods, between-neuron timing
801 information is lost when transforming the neuronal spiking time series to cross-correlation matrices.
802 Apart from losing the specification of the order and timing of the network spiking sequence, this also
803 makes it more difficult to distinguish between those networks that involve the same neurons, but at
804 different between-neuron spike times. This adds unto the rotational ambiguity of PCA that influences
805 network identification and separation, although (Lopes-dos-Santos et al., 2011) made significant
806 advances with respect to the latter. In comparison, the method behind our approach (van der Meij et
807 al., 2015), and related methods (Harshman and Lundy, 1994; Bro, 1998; Kiers et al., 1999; Sidiropoulos
808 et al., 2000; Morup et al., 2008), extracts networks that are unique without rotational ambiguity, and
809 separates them on the basis of their different structure across neurons, frequencies, and trials. Several
810 other approaches use cross-correlation matrices in way that did allow for an investigation of between-
811 neuron spiking at time delays (Schneider et al., 2006; Nikolic, 2007; Humphries, 2011), but these
812 approaches were not targeted at identifying and separating networks and their spiking sequences.

813 In summary, we have presented an approach that can extract networks defined by their
814 between-neuron spike timing consistency, with arbitrary network size and high temporal precision of
815 the identified spike sequences. Especially the latter is important considering the growing number of
816 neurons that can be recorded simultaneously, and the complexity of spike sequences that can thus be
817 measured. Ultimately, the usefulness of our approach and those related to it, lies in whether spike
818 timing plays a crucial role in large, distributed, neuronal networks. Being able to search for these
819 networks with increased sensitivity is essential to the investigation of their existence and function.

820 **References**

- 821
- 822 Abeles M, Gerstein GL (1988) Detecting spatiotemporal firing patterns among simultaneously recorded
823 single neurons. *J Neurophysiol* 60:909–924.
- 824 Ainsworth M, Lee S, Cunningham MO, Traub RD, Kopell NJ, Whittington MA (2012) Rates and Rhythms:
825 A Synergistic View of Frequency and Temporal Coding in Neuronal Networks. *Neuron* 75:572–583.
- 826 Balaguer-Ballester E, Lapish CC, Seamans JK, Durstewitz D (2011) Attracting Dynamics of Frontal Cortex
827 Ensembles during Memory-Guided Decision-Making. *PLOS Comput Biol* 7.
- 828 Berger D, Borgelt C, Louis S, Morrison A, Grün S (2010) Efficient Identification of Assembly Neurons
829 Within Massively Parallel Spike Trains. *Intell Neurosci* 2010:1:1--1:18.
- 830 Bienenstock E (1995) A model of neocortex. *Netw Comput neural Syst* 6:179–224.
- 831 Bro R (1998) Multi-way Analysis in the Food Industry. Models, Algorithms, and Applications. PhD.
- 832 Brosch M, Schreiner CE (1999) Correlations between neural discharges are related to receptive field
833 properties in cat primary auditory cortex. *Eur J Neurosci* 11:3517–3530.
- 834 Buzsaki G (2004) Large-scale recording of neuronal ensembles. *Nat Neurosci* 7:446–451.
- 835 Buzsaki G (2010) Neural Syntax: Cell Assemblies, Synapsembles, and Readers. *Neuron* 68:362–385.
- 836 Chapin JK, Nicolelis MAL (1999) Principal component analysis of neuronal ensemble activity reveals
837 multidimensional somatosensory representations. *J Neurosci Methods* 94:121–140.
- 838 Comon P, ten Berge JMF, Lathauwer L De, Castaing J (2009) Generic and typical ranks of multi-way
839 arrays. *Linear Algebra Appl* 430:2997–3007.
- 840 Eldawlatly S, Zhou Y, Jin R, Oweiss KG (2010) On the Use of Dynamic Bayesian Networks in
841 Reconstructing Functional Neuronal Networks from Spike Train Ensembles. *NEURAL Comput*
842 22:158–189.
- 843 Feldman DE (2012) The Spike-Timing Dependence of Plasticity. *Neuron* 75:556–571.
- 844 Fujisawa S, Amarasingham A, Harrison MT, Buzsaki G (2008) Behavior-dependent short-term assembly
845 dynamics in the medial prefrontal cortex. *Nat Neurosci* 11:823–833.
- 846 Fujisawa S, Amarasingham A, Harrison MT, Buzsáki G (2014) Simultaneous electrophysiological
847 recordings of ensembles of isolated neurons in rat medial prefrontal cortex and intermediate CA1
848 area of the hippocampus during a working memory task.
- 849 Gansel K, Singer W (2012) Detecting Multineuronal Temporal Patterns in Parallel Spike Trains. *Front
850 Neuroinform* 6:18.
- 851 Gochin PM, Miller EK, Gross CG, Gerstein GL (1991) Functional interactions among neurons in inferior
852 temporal cortex of the awake macaque. *Exp Brain Res* 84:505–516.
- 853 Grün S (2009) Data-Driven Significance Estimation for Precise Spike Correlation. *J Neurophysiol* 101:1126
854 LP-1140.
- 855 Grün S, Diesmann M, Aertsen A (2002) Unitary Events in Multiple Single-Neuron Spiking Activity: I.
856 Detection and Significance. *Neural Comput* 14:43–80.
- 857 Harris KD (2005) Neural signatures of cell assembly organization. *Nat Rev Neurosci* 6:399–407.
- 858 Harshman RA, Lundy ME (1994) PARAFAC: Parallel factor analysis. *Comput Stat Data Anal* 18:39–72.
- 859 Hebb D. (1949) The Organization of Behavior. A neuropsychological theory.
- 860 Humphries MD (2011) Spike-Train Communities: Finding Groups of Similar Spike Trains. *J Neurosci*
861 31:2321–2336.
- 862 Ikegaya Y, Aaron G, Cossart R, Aronov D, Lampl I, Ferster D, Yuste R (2004) Synfire chains and cortical
863 songs: temporal modules of cortical activity. *Science* (80-) 304:559–564.
- 864 Izhikevich EM (2006) Polychronization: computation with spikes. *Neural Comput* 18:245–282.
- 865 Kiers HAL, Ten Berge JMF, Bro R (1999) PARAFAC2 - Part I. A direct fitting algorithm for the PARAFAC2
866 model. *J Chemom* 13:275–294.
- 867 Kreiter AK, Singer W (1996) Stimulus-dependent synchronization of neuronal responses in the visual

- 868 cortex of the awake macaque monkey. *J Neurosci* 16:2381–2396.
- 869 Kumar A, Rotter S, Aertsen A (2010) Spiking activity propagation in neuronal networks: reconciling
870 different perspectives on neural coding. *Nat Rev Neurosci* 11:615.
- 871 Lee AK, Wilson MA (2002) Memory of sequential experience in the hippocampus during slow wave
872 sleep. *Neuron* 36:1183–1194.
- 873 Lindemann M, Raethjen J, Timmer J, Deuschl G, Pfister G (2001) Delay estimation for cortico-peripheral
874 relations. *J Neurosci Methods* 111:127–139.
- 875 Lopes-dos-Santos V, Conde-Ocazinez S, Nicolelis MAL, Ribeiro ST, Tort ABL (2011) Neuronal Assembly
876 Detection and Cell Membership Specification by Principal Component Analysis. *PLoS One* 6.
- 877 Louis S, Borgelt C, Gruen S (2010) Complexity distribution as a measure for assembly size and temporal
878 precision. *NEURAL NETWORKS* 23:705–712.
- 879 Luczak A, Barthó P, Marguet SL, Buzsáki G, Harris KD (2007) Sequential structure of neocortical
880 spontaneous activity in vivo. *Proc Natl Acad Sci* 104:347–352.
- 881 MacLean JN, Watson BO, Aaron GB, Yuste R (2005) Internal Dynamics Determine the Cortical Response
882 to Thalamic Stimulation. *Neuron* 48:811–823.
- 883 Mainen ZF, Sejnowski TJ (1995) Reliability of Spike Timing in Neocortical Neurons. *Science* (80-)
884 268:1503–1506.
- 885 Mao BQ, Hamzei-Sichani F, Aronov D, Froemke RC, Yuste R (2001) Dynamics of spontaneous activity in
886 neocortical slices. *Neuron* 32:883–898.
- 887 Matsumoto K, Ishikawa T, Matsuki N, Ikegaya Y (2013) Multineuronal spike sequences repeat with
888 millisecond precision. *Front Neural Circuits* 7:112.
- 889 Miller JK, Ayzenshtat I, Carrillo-Reid L, Yuste R (2014) Visual stimuli recruit intrinsically generated cortical
890 ensembles. *Proc Natl Acad Sci U S A* 111:E4053–E4061.
- 891 Morup M, Hansen LK, Arnfred SM, Lim LH, Madsen KH (2008) Shift-invariant multilinear decomposition
892 of neuroimaging data. *Neuroimage* 42:1439–1450.
- 893 Nadasdy Z, Hirase H, Czurko A, Csicsvari J, Buzsaki G (1999) Replay and time compression of recurring
894 spike sequences in the hippocampus. *J Neurosci* 19:9497–9507.
- 895 Nakahara H, Amari S (2002) Information-geometric measure for neural spikes. *NEURAL Comput*
896 14:2269–2316.
- 897 Nelson JL, Salin PA, Munk MH-J, Arzi M, Bullier J (1992) Spatial and temporal coherence in cortico-
898 cortical connections: A cross-correlation study in areas 17 and 18 in the cat. *Vis Neurosci* 9:21–37.
- 899 Nikolic D (2007) Non-parametric detection of temporal order across pairwise measurements of time
900 delays. *J Comput Neurosci* 22:5–19.
- 901 Okatan M, Wilson MA, Brown EN (2005) Analyzing functional connectivity using a network likelihood
902 model of ensemble neural spiking activity. *NEURAL Comput* 17:1927–1961.
- 903 Panzeri S, Brunel N, Logothetis NK, Kayser C (2010) Sensory neural codes using multiplexed temporal
904 scales. *Trends Neurosci* 33:111–120.
- 905 Peyrache A, Benchenane K, Khamassi M, Wiener SI, Battaglia FP (2010) Principal component analysis of
906 ensemble recordings reveals cell assemblies at high temporal resolution. *J Comput Neurosci*
907 29:309–325.
- 908 Pipa G, Wheeler DW, Singer W, Nikolic D (2008) NeuroXidence: reliable and efficient analysis of an
909 excess or deficiency of joint-spike events. *J Comput Neurosci* 25:64–88.
- 910 Ratté S, Hong S, De Schutter E, Prescott SA (2013) Impact of Neuronal Properties on Network Coding:
911 Roles of Spike Initiation Dynamics and Robust Synchrony Transfer. *Neuron* 78:758–772.
- 912 Rolls ET, Treves A (2011) The neuronal encoding of information in the brain. *Prog Neurobiol* 95:448–490.
- 913 Rossant C, Kadir SN, Goodman DFM, Schulman J, Hunter MLD, Saleem AB, Grosmark A, Belluscio M,
914 Denfield GH, Ecker AS, Tolias AS, Solomon S, Buzsaki G, Carandini M, Harris KD (2016) Spike sorting
915 for large, dense electrode arrays. *Nat Neurosci* 19:634–641.

- 916 Sakurai Y, Nakazono T, Ishino S, Terada S, Yamaguchi K, Takahashi S (2013) Diverse synchrony of firing
917 reflects diverse cell-assembly coding in the prefrontal cortex. *J Physiol* 107:459–470.
- 918 Salinas E, Sejnowski TJ (2001) Correlated neuronal activity and the flow of neural information. *Nat Rev
919 Neurosci* 2:539–550.
- 920 Schneider G, Havenith MN, Nikolic D (2006) Spatiotemporal structure in large neuronal networks
921 detected from cross-correlation. *NEURAL Comput* 18:2387–2413.
- 922 Schnitzer MJ, Meister M (2003) Multineuronal firing patterns in the signal from eye to brain. *Neuron*
923 37:499–511.
- 924 Schrader S, Grün S, Diesmann M, Gerstein GL (2008) Detecting Synfire Chain Activity Using Massively
925 Parallel Spike Train Recording. *J Neurophysiol* 100:2165–2176.
- 926 Shimazaki H, Amari S, Brown EN, Gruen S (2012) State-Space Analysis of Time-Varying Higher-Order
927 Spike Correlation for Multiple Neural Spike Train Data. *PLOS Comput Biol* 8.
- 928 Sidiropoulos ND, Giannakis GB, Bro R (2000) Blind PARAFAC receivers for DS-CDMA systems. *IEEE Trans
929 Signal Process* 48:810–823.
- 930 Singer W (1999) Neuronal synchrony: A versatile code for the definition of relations? *Neuron* 24:49–65.
- 931 Staude B, Rotter S, Gruen S (2010) CuBIC: cumulant based inference of higher-order correlations in
932 massively parallel spike trains. *J Comput Neurosci* 29:327–350.
- 933 Tetko I V, Villa AEP (2001) A pattern grouping algorithm for analysis of spatiotemporal patterns in
934 neuronal spike trains. 1. Detection of repeated patterns. *J Neurosci Methods* 105:1–14.
- 935 Tiesinga P, Fellous JM, Sejnowski TJ (2008) Regulation of spike timing in visual cortical circuits. *Nat Rev
936 Neurosci* 9:97–109.
- 937 Torre E, Canova C, Denker M, Gerstein G, Helias M, Gruen S (2016) ASSET: Analysis of Sequences of
938 Synchronous Events in Massively Parallel Spike Trains. *PLOS Comput Biol* 12.
- 939 Treisman A (1996) The binding problem. *Curr Opin Neurobiol* 6:171–178.
- 940 van der Meij R, Jacobs J, Maris E (2015) Uncovering phase-coupled oscillatory networks in
941 electrophysiological data. *Hum Brain Mapp* 36:2655–2680.
- 942 van der Meij R, van Ede F, Maris E (2016) Rhythmic Components in Extracranial Brain Signals Reveal
943 Multifaceted Task Modulation of Overlapping Neuronal Activity. *PLoS One* 11:e0154881.
- 944 VanRullen R, Guyonneau R, Thorpe SJ (2005) Spike times make sense. *Trends Neurosci* 28:1–4.
- 945 Varela F, Lachaux JP, Rodriguez E, Martinerie J (2001) The brainweb: Phase synchronization and large-
946 scale integration. *Nat Rev Neurosci* 2:229–239.
- 947 Yu BM, Cunningham JP, Santhanam G, Ryu SI, Shenoy K V, Sahani M (2009) Gaussian-Process Factor
948 Analysis for Low-Dimensional Single-Trial Analysis of Neural Population Activity. *J Neurophysiol*
949 102:614–635.
- 950
- 951
- 952
- 953

954

Figure captions

955

956 **Figure 1. Schematic of extracting spike timing networks.** Neuronal spiking time series can contain
957 consistent spike timing between neurons, forming spike sequences. **A**, schematic of two spike timing
958 networks, with their neurons (circles) and sequence spikes (vertical lines) colored blue and green. The
959 dashed lines reflect the between-neuron consistent spike time relationships resulting from the spike
960 sequences. The blue network's sequence goes from neuron 3 to 4 to 5 (dark dashed lines), with 1ms
961 time delays, resulting in a 2ms delay from 3 to 5 (light dashed line). The green network's sequence is the
962 same but from neuron 5 to 6 to 7. **B**, the spike time consistencies in A can also be visualized as cross-
963 correlograms between all neuron pairs, at lags ranging from -10ms to 10ms with 1ms bins. **C**, the
964 networks in A and B but shown as spike trains per trial of two experimental conditions. The blue
965 network trials' have one sequence in condition A and two sequences in condition B, vice versa for the
966 green network. To extract these two networks, we arrange spike trains of all neurons in a neuron-by-
967 time binary matrix. These spike trains are then convolved with complex exponentials (or 'wavelets') of
968 equal length at different frequencies, resulting in a complex-valued neuron-by-time matrix per
969 frequency per trial. **D**, the cross products are then computed along the time dimension, resulting in a
970 neuron-by-neuron cross-product matrix per frequency per trial: the cross spectrum. The between-
971 neuron phase differences of the cross spectra over frequencies, reflect the consistent between-neuron
972 spike time delays. **E**, using a recent technique denoted as SPACE, the structure in the cross spectra over
973 frequencies can be extracted, and described as separate spike timing networks. The blue and green
974 networks are each described by a neuron profile, describing network membership by a single weight per
975 neuron, a time profile, describing the spike sequence by a time coefficient per neuron, and a trial profile,
976 having a single weight per trial, indicating how strongly the network was present. For details see
977 Materials and Methods section 1, 2, 3.

978

979 **Figure 2. Simulated spike timing networks.** To investigate the robustness of network extraction to
980 various kinds of noise we simulated spike recordings from 15 neurons containing 4 spike timing
981 networks across 100 trials. **A-C**, description of simulated networks in same format as extracted
982 networks. **A**, the neuron profile of each network describes non-member neurons by 0s and member
983 neurons by 1s. Because absolute magnitudes of the neuron and trial profiles of networks are not
984 meaningful, they are L2-normalized by convention (leading to the visible arbitrary between-network
985 amplitude differences); the between-neuron/trial *ratios* are meaningful. **B**, the spiking sequence of each
986 network, shown as their time profiles (only member neurons are shown). **C**, the trial profile. Each
987 network spiking sequence was repeated 0-3 times in each trial, shown per trial in the first row. The
988 second row of C shows an alternative visualization of the trial profile, which is convenient for visualizing
989 recovery (see Fig 3-6). Here, normalized trial profile weights (y-axis) are shown as their mean (SD), per
990 simulated number of spike sequence repeats (x-axis). **D**, schematic of all consistent spike timing
991 relationships resulting from the simulated spike sequences. Each circle is a neuron, each dashed line
992 reflects a spike timing relationship. For visibility, the first-order relationships are dark colored, all others
993 are light colored. Numbers indicate the first-order within-sequence spike time delays. **E**, cross-
994 correlograms computed for all neuron-pairs from a simulation run with 20Hz spiking noise, at lags
995 ranging from -10ms to 10ms with 1ms bins. **F**, raster plots of example spike trains as a function of
996 spiking noise levels used in the simulations. Each vertical dash is a single spike. Each row consists of 5
997 concatenated trials, separated by a vertical line. Network spiking sequences are shown by their color as
998 in A-D. See Materials and Methods section 5.

999

1000 **Figure 3. Recovery of simulated spike timing networks with spiking jitter and spiking noise.** Networks
1001 were simulated 50 times at 5 levels of spiking jitter and 5 levels of spiking noise. Recovery of the neuron

1002 and trial profiles are shown as Pearson correlations between the extracted and simulated networks
1003 (ranged from -1 to 1, visualized from 0 to 1; averaged over simulations; shading = SEM). The recovery of
1004 the time profile is shown by a recovery coefficient ranging from 0 to 1 (perfect recovery; averaged over
1005 simulations; shading = SEM). Networks are colored as in Figure 2. Bottom panels visualize extracted
1006 networks as in Figure 2 at several example jitter and noise levels. Neuron profiles are shown as means
1007 over simulations (shading = SD), with that of individual simulations as thin lines. Time profiles are
1008 displayed as average over simulations (error bar = SD; aligned using average difference between
1009 simulated and recovered networks). Trial profiles show means over trial weights per # of simulated
1010 sequence repeats, averaged over simulations (error bar = SD). The simulated trial profiles and time
1011 profiles are indicated in gray for reference. Note that, (1) when spiking noise and jitter increased, the
1012 trial profiles 'baseline' (weights of non-contributing trials that should be 0) gradually increased, (2)
1013 spiking noise had a stronger effect on the trial profiles of networks with fewer neurons, and, (3) the time
1014 profiles were more robust to noise than the neuron profiles and trial profiles, with accurate recovery
1015 even when spike jitter was a multiple of the between-neuron time delays. Also note in the examples
1016 that as noise increased, matching of simulated networks to extracted networks became troublesome,
1017 leading to differences between network-specific recovery becoming less meaningful. See Materials and
1018 Methods section 5 and 6.
1019

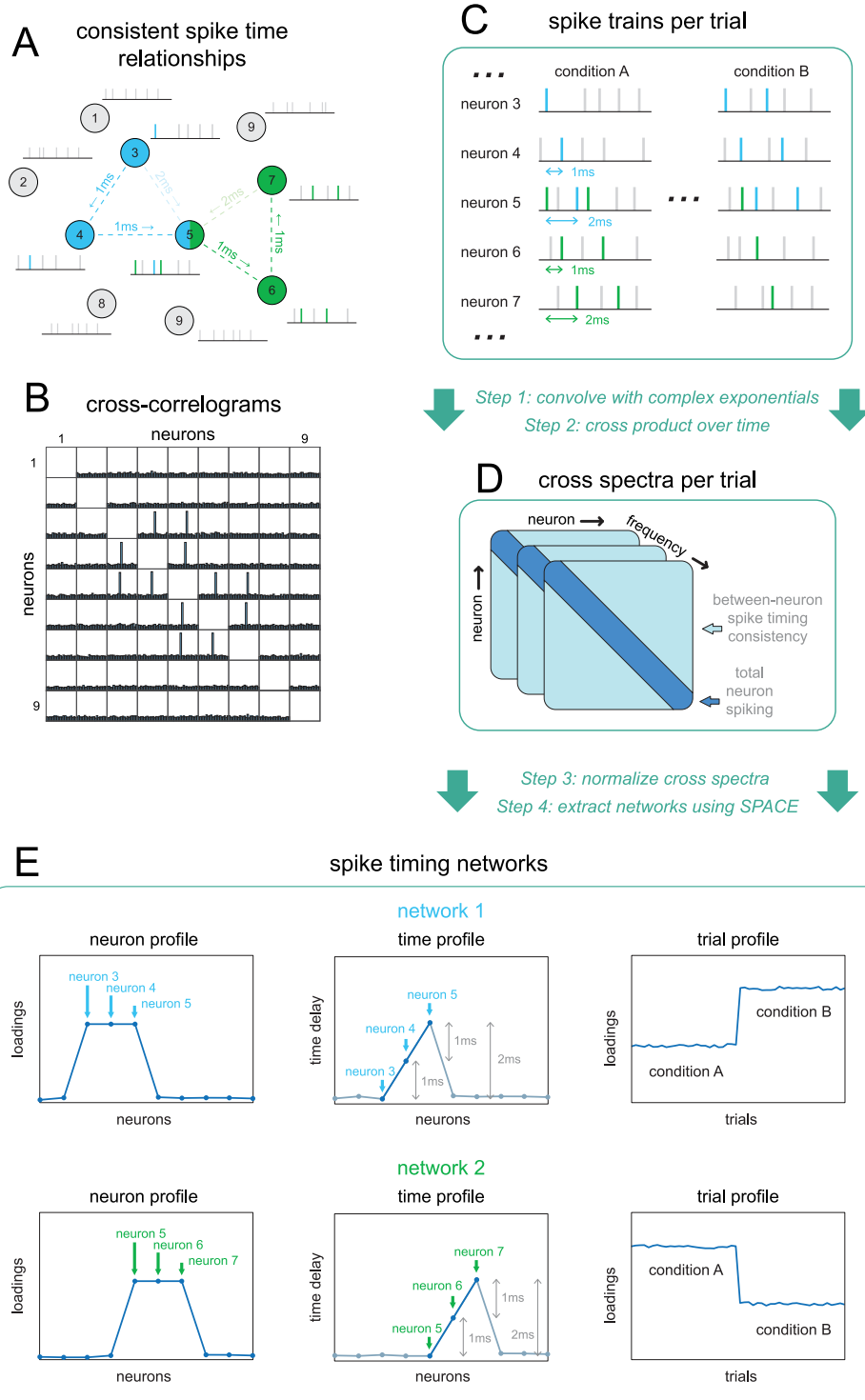
1020 **Figure 4. Recovery of simulated spike timing networks with partial network spiking and spiking noise.**
1021 Networks were simulated 50 times at 5 probability levels of spike deletion, and 5 levels of spiking noise.
1022 Probability is the chance for each individual (non-noise) spike to be deleted. Recovery and examples are
1023 displayed identically to Figure 3. Note that, (1) the effect of spike deletion affected the neuron profiles,
1024 time profiles, and trial profiles similarly to that of spike jitter and spiking noise, and, (2) even when the
1025 spiking sequences of the networks were highly variable (80% chance of each spike's absence) the
1026 networks could still be identified in the examples at 5Hz spiking noise. See Materials and Methods
1027 section 5 and 6.
1028

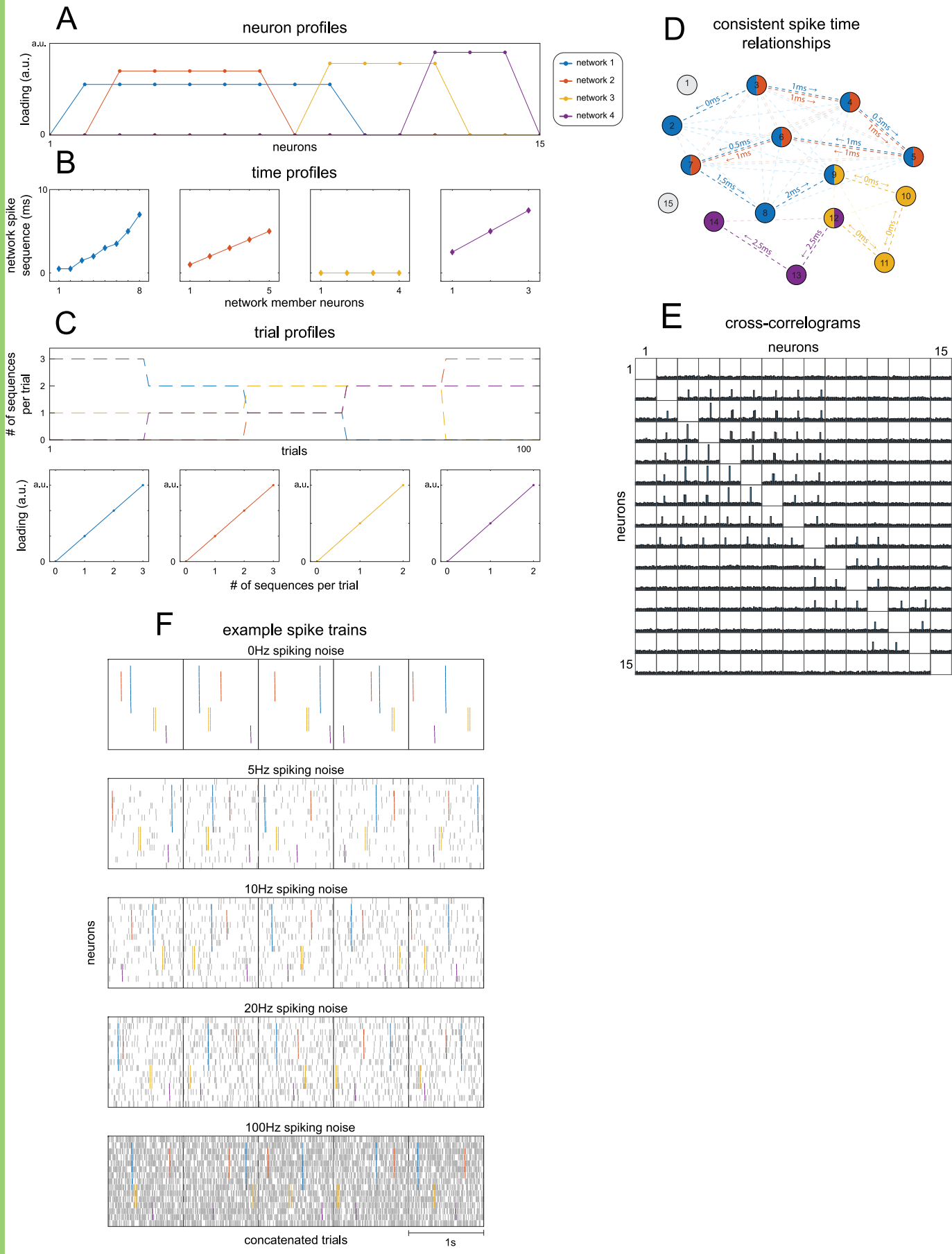
1029 **Figure 5. Cross spectra normalization diminishes effects of differential neuron firing rates.** In realistic
1030 neuron recordings, the firing rate of neurons typically differ. To show the effect of differential firing
1031 rates on network recovery, we simulated spike timing networks (spiking jitter = ± 0.25 ms; spike deletion
1032 = 10%) 50 times with two neurons having 100Hz spiking noise, the other neurons 5Hz. To improve
1033 network recovery, the cross spectra can be normalized. One method is to normalize them such that the
1034 power of the cross spectra becomes equal to their Nth root. **A**, spiking noise as a function of neurons,
1035 with the simulated neuron profiles in the background. **B**, network recovery without normalization.
1036 Though the networks are recognizable, recovery was clearly affected. Networks are displayed identically
1037 to examples in Figure 3. **C**, the effect of square, 4th, 8th, 16th, 32nd root power normalization on recovered
1038 networks, culminating in: **D**, recovered networks after 64th-root power normalization. See Materials and
1039 Methods section 4 and 5.
1040

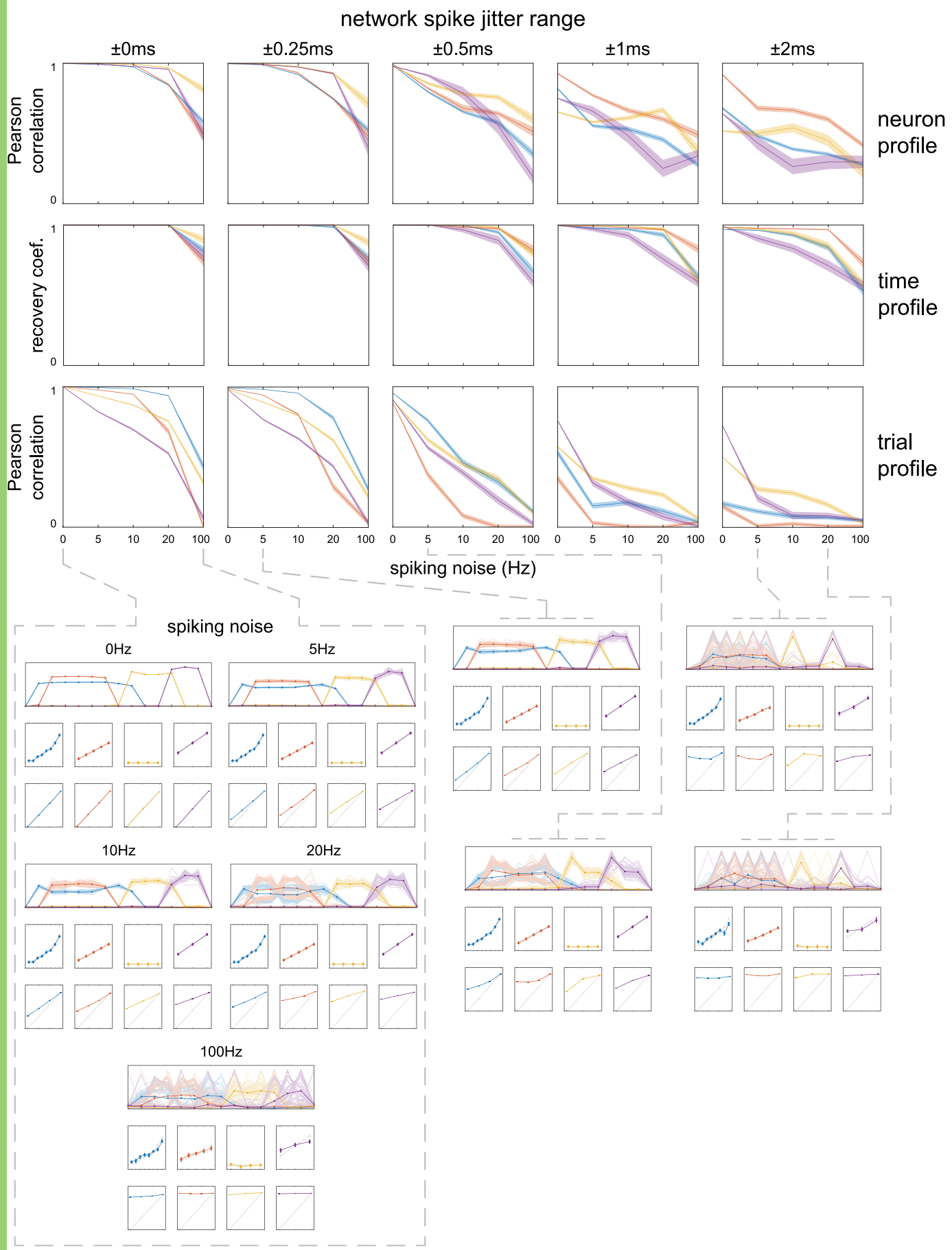
1041 **Figure 6. Trial-wise cross spectra normalization diminishes effects of differential trial firing rates.** In
1042 realistic recordings, the firing rate of neurons can differ over trials. To show its effect on network
1043 recovery, we simulated spike timing networks (spiking jitter = ± 0.25 ms; spike deletion = 10%) 50 times
1044 with 40 trials having 10Hz spiking noise (for all neurons), the other trials 5Hz. To improve network
1045 recovery, the cross spectra can be normalized in a similar way as for differential neuron firing rates.
1046 Here, we normalize the cross spectra of each trial such that their power is equal to that summed over
1047 trials. **A**, spiking noise as a function of trials, with the simulated trial profiles in the background. **B**,
1048 recovered networks with trial-wise normalization. Networks are displayed identically to examples in
1049 Figure 3. The trial profiles of the recovered networks were strongly affected. **C**, like B but for networks

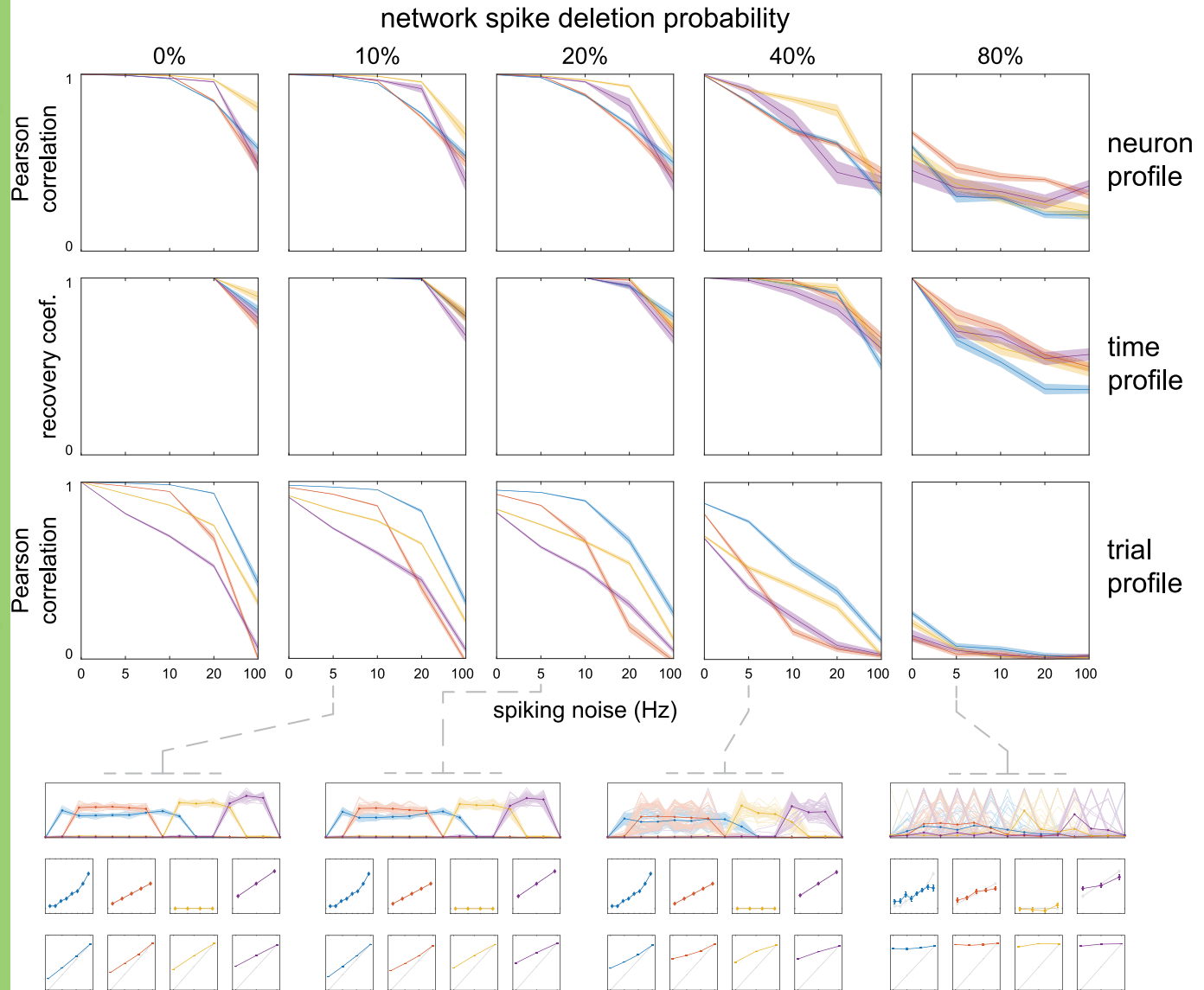
1050 recovered after trial-wise normalization. While the trial profiles still deviated from the simulated
1051 networks, the ratios of their weights w.r.t. the # of simulated sequence repeats were partially restored.
1052 See Materials and Methods section 4 and 5.

1053
1054 **Figure 7. Example spike timing networks extracted from rat medial prefrontal cortex and**
1055 **hippocampus.** We extracted 4 spike timing networks from recordings in which a rat either had to take
1056 the left or right arm of a figure-eight T-maze. The number of networks to extract was estimated using a
1057 split-half approach. The first row of each network shows the neuron profile, the time profile, and the
1058 trial profile. The time profile only shows the strongest 5 neurons of the trial profile (as given by the
1059 neuron profile). Several of the strongest neurons are highlighted in each neuron profile. To show that
1060 the networks reflect spike timing consistencies in the data, we also show cross-correlograms in the
1061 second and third row. The cross-correlograms of each pair of the highlighted neurons are shown as spike
1062 densities, the y-axis limit roughly reflects spike counts. The dashed gray line is the time delay between
1063 the neurons as given by the time profile of the network. We observe the following. For network 1,
1064 neuron pairs 1-2, 1-3, and 2-3 the extracted time delays are close to the cross-correlogram. Though the
1065 4th neuron has a higher weight than the non-highlighted neurons in the neuron profile, the cross-
1066 correlograms are not as strongly peaked as for the other pairs. For network 2, the extracted time delays
1067 of pairs 1-2, 1-3, 1-4 are closest to their cross-correlograms. Though for network 3 the cross-
1068 correlograms show weaker spike timing consistency (higher baseline spike density), the extracted time
1069 delays of pair 1-2, 1-3, 1-4, and 2-3 are close to their peaks. Network 4 involves few strong neurons, as
1070 indicated by the neuron profile; only the neuron pair 1-2 is close to its peak. See Materials and Methods
1071 section 7.

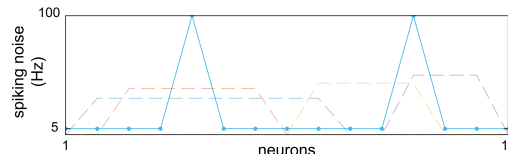




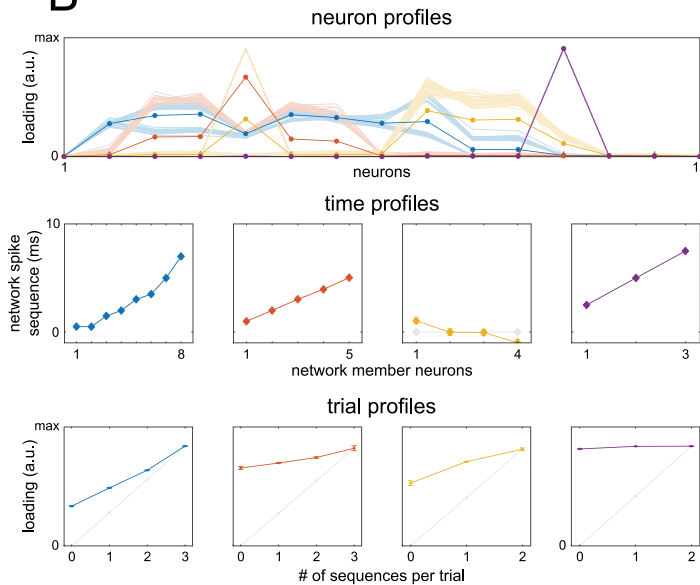




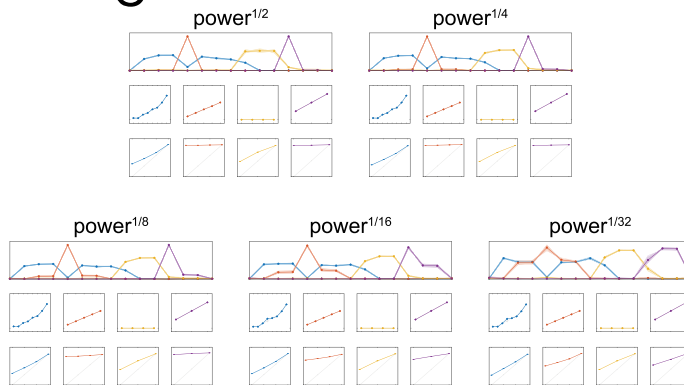
A neuron-specific spiking noise



B no normalization



C normalization: power =



D normalization: power = power^{1/64}

